Quarterly Technical Report

Defects and Impurities in 4H- and 6H-SiC Homoepitaxial Layers: Identification, Origin, Effect on Properties of Ohmic Contacts and Insulating Layers and Reduction

Supported under Grant #N00014-95-1-1080
Office of the Chief of Naval Research
Report for the period 10/1/95–12/31/95

R. F. Davis, M. O. Aboelfotoh, B. J. Baliga*, R. J. Nemanich†,
P. K. McLarty*, S. Fleming, S. King, M. O'Brien†, L. S. Porter,
R. Raghunathan*, S. Sridevan*, and H. S. Tomozawa
Department of Materials Science and Engineering
*Department of Electrical and Computer Engineering
†Department of Physics
North Carolina State University
Campus Box 7907
Raleigh, NC 27695-7907

December, 1995

REPORT DOCUMENTATION PAGE

Form Approved
OMB No. 0704-0188

1. AGENCY USE ONLY *(Leave blank)*	2. REPORT DATE	3. REPORT TYPE AND DATES COVERED
	December, 1995	Quarterly Technical 10/1/95–12/31/95

4. TITLE AND SUBTITLE
Defects and Impurities in 4H- and 6H-SiC Homoepitaxial Layers: Identification, Origin, Effect on Properties of Ohmic Contacts and Insulating Layers and Reduction

5. FUNDING NUMBERS
ydl4951---01
312
N00179
N66020
4B855

6. AUTHOR(S)
R. F. Davis, M. O. Aboelfotoh, B. J. Baliga and R. J. Nemanich

7. PERFORMING ORGANIZATION NAME(S) AND ADDRESS(ES)
North Carolina State University
Hillsborough Street
Raleigh, NC 27695

8. PERFORMING ORGANIZATION REPORT NUMBER
N00014-95-1-1080

9. SPONSORING/MONITORING AGENCY NAMES(S) AND ADDRESS(ES)
Sponsoring: ONR, Code 312, 800 N. Quincy, Arlington, VA 22217-5660
Monitoring: Administrative Contracting Officer, Regional Office Atlanta
Regional Office Atlanta, 101 Marietta Tower, Suite 2805
101 Marietta Street
Atlanta, GA 30323-0008

10. SPONSORING/MONITORING AGENCY REPORT NUMBER

11. SUPPLEMENTARY NOTES

12a. DISTRIBUTION/AVAILABILITY STATEMENT
Approved for Public Release; Distribution Unlimited

12b. DISTRIBUTION CODE

13. ABSTRACT ***(Maximum 200 words)***

A deposition system containing a separate load lock and attached growth and RHEED chambers has been designed for the growth of undoped and doped 4H- and 6H-SiC thin films. Several *ex situ* techniques were examined for cleaning 6H-SiC(0001)$_{Si}$, (000-1)$_{C}$, (11-20), and (10-10) surfaces. The wetting characteristics of SiC in various acids and bases, e.g., HF, HCl, H_2SO_4, HNO_3, acetic, lactic, NH_3OH, NH_4F, and H_2O_2 were examined and compared. Silicon carbide surfaces dipped in all acids or bases were hydrophilic. Similar levels of oxygen were detected on all surface orientations after exposure to HF, NH_4F, HF:NH_4F mixtures or HF with the pH adjusted with HCl or NH_3OH. Silicon carbide surfaces coated with 20-50Å of Si exhibited wetting characteristics after HF dipping similar to that of Si (111). All 6H-SiC(0001)$_{Si}$, (11-20), and (10-10) surfaces exhibited similar C/Si and C/O levels. The 6H-SiC (000-1)$_{C}$ surface exhibited slightly larger C/Si ratios after HF dipping. UV/ozone oxidation of the SiC surface using a Hg lamp was investigated and found capable of oxidizing the SiC surface but was not successful in completely removing all of the non-carbidic carbon from the SiC surfaces. However, XPS studies revealed that the UV/ozone treatment did change the chemical state of the non-carbidic C. This was seen via a shift in the non-carbidic C 1s from 285.7 to 285.2 eV. An integrated, UHV compatible system is also being developed for integrated *in situ* cleaning, oxidation and oxide deposition on 6H- and 4H-SiC. The cleaning capabilities will include H-plasma, SiH_4 dosing, and *in situ* vapor phase HF cleaning. Oxide formation will involve multi-step processing including plasma oxidation, plasma CVD, UHV thermal oxidation, and UHV CVD. A mask set has been designed and purchased to fabricate MOS capacitors that will enable accurate characterization of the SiO_2-SiC interface. The process flow to be used in the fabrication and characterization of these devices is outlined. Diffusion lengths of the minority carriers in 6H- and 4H-SiC have been measured using a Schottky barrier diode and SEM in the EBIC mode. The values in n-type 6H-SiC and n-type 4H-SiC were ≈0.4 μm and ≈1.4 μm, respectively. Using these values the minority carrier lifetimes were estimated to be 0.65 nsec in 6H-SiC and 5.6 nsecs in 4H-SiC. As-deposited (at RT) NiAl contacts with Ni passivating layers on p-type 6H-SiC(0001) substrates were rectifying with very low ρ_L (~1×10^{-8} A/cm^2 at 10 V), I_D values between 1.4 and 2.4, and a SBH of ≈1.37 eV. As-deposited (at RT) Ni and Au contacts on p-type 6H-SiC displayed similar C-V characteristics with SBH values of 1.31 and 1.27 eV, respectively. The Fermi level is partially pinned in p-type 6H-SiC. The Ni/NiAl contacts on p$^+$ (1×10^{19} cm^{-3}) 6H-SiC (0001) were ohmic after annealing for 10–80 s at 1000°C in a N_2 ambient. The estimated specific contact resistivity from a non-mesa etched TLM pattern was 2–3×10^{-2} W•cm^{-2}. Several boron compounds were selected as alternatives to Al materials.

14. SUBJECT TERMS
silicon carbide, SiC, 6H-SiC, 4H-SiC, chemical vapor deposition, CVD, cleaning, surfaces, acids, bases, UV/ozone oxidation, XPS, H-plasma, oxidation, plasma oxidation, MOS capacitors, diffusion lengths, minority carrier, NiAl alloys, Ni, Al, rectifying, ohmic, Schottky barrier height, contact resistivity, leakage current, Fermi level, boron

15. NUMBER OF PAGES
49

16. PRICE CODE

17. SECURITY CLASSIFICATION OF REPORT	18. SECURITY CLASSIFICATION OF THIS PAGE	19. SECURITY CLASSIFICATION OF ABSTRACT	20. LIMITATION OF ABSTRACT
UNCLAS	UNCLAS	UNCLAS	SAR

Table of Contents

I. Introduction

The two most important materials-related problems affecting the performance of all SiC devices and their associated components (e.g., contacts) are the defects and the undesired impurities which become incorporated in the homoepitaxial SiC layers in which all devices are currently fabricated. Bhatnagar [1] has shown that the reverse blocking leakage current in high voltage Schottky diodes is three orders of magnitude higher than theoretically predicted as a result of defects in the epi-layer. The formation of micropipes, stepped screw dislocations, interacting dislocation loops, polyganized networks of dislocations and growth twins as well as stacking faults during the sublimation growth of SiC boules are likely the root cause of some of the defects in the epitaxial layer. However, with the exception of the micropipes, the types and concentrations of line, planar and other three-dimensional defects and their effect on the performance of devices and individual device components in the important epi-layer have not been similarly determined. As such, it is not known which of the latter defects actually are translated from the wafer into the epi-layer during its deposition and, therefore, should be vigorously controlled during boule growth and which defects are generated during deposition.

The relatively uncontrolled occurrence of the n-type donor of N and deep level compensating impurities such as Ti in the epilayer have been identified via secondary ion mass spectrometry, photoluminescence and cathodoluminescence investigations. However, the origins of essentially all of these impurities are unknown. For high-temperature, -power and -frequency devices, it is highly desirable to control or eliminate these impurities such as to attain undoped films with uncompensated carrier concentrations of 10^{14} cm^{-3}—two orders of magnitude lower than what is, at present, normally achieved in standard commercial depositions.

The formation of low resistivity and thermally stable ohmic contacts to 4H- and 6H-SiC remains a serious problem in the development of SiC device technology. For SiC power devices to have an advantage over Si, the contact resistivities must be below 1×10^{-5} Ω-cm^2, as noted by Alok, *et al.* [2]. In addition, the electrical characterization of state-of-the-art SiC films depends on the ability to fabricate ohmic contacts on material with low carrier concentrations. Therefore, better ohmic contacts are needed both for improving device performance and for improving the quality of films which can be grown. The thermal stability of ohmic contacts is of particular concern for p-type SiC, which have traditionally relied on low melting point Al or Al alloys to dope the SiC surface below the contacts. These materials are not suitable for devices intended for high-temperature operation. While the fabrication of ohmic contacts to SiC has also normally depended on the attainment of a very heavily-doped near-surface region, the introduction during deposition of high levels of dopants in the near surface device region of the epi-layer prior to the deposition of the contact or by ion implantation through the contact makes probable the introduction of point and line defects as a result of the induced strain in the lattice.

Based on all of these issues and recent experiments already performed at NCSU, our goals are to produce contacts which are thermally stable and have low contact resistivities while also reducing the need for doping by ion implantation.

To fabricate most microelectronic devices, the growth or deposition of stable insulators is needed to provide both passivating layers and gate dielectrics. Silicon carbide is almost invariably thermally oxidized, albeit at a slower rate, in the same manner and temperature range that is employed for Si. Most of the previous studies regarding the oxidation of SiC have been concerned with polycrystalline materials. It has been shown by Harris and Call [3] and Suzuki, *et al.* [4] that the (0001) face of 6H-SiC oxidizes according to the same linear-parabolic equation reported for Si by Deal and Grove [5]. The model states that the initial stage of oxidation is reaction rate limited and linear, but becomes parabolic as the diffusion of the oxidant through the oxide becomes the rate limiting factor. Research at NCSU by Palmour *et al.* [6] has demonstrated that the oxidation process on SiC in wet and dry oxygen and wet argon obeys the linear-parabolic law. Both wet processes had a slower rate than dry oxidation at 1050°C and below. The dry oxides exhibited a very flat surface; in contrast, SEM and TEM revealed that wet oxidation preferentially oxidizes dislocation bands, causing raised lines on the oxide and corresponding grooves in the SiC. It was proposed that the much higher solubility of H_2O in SiO_2 as compared to that of O_2 allows wet oxidation to be preferential.

All of the oxidation studies on all polytypes of semiconductor quality SiC have been conducted on n-type material with the exception of the investigation by Palmour *et al.* [6]. The objective of this study was the determination of the redistribution of the common electrical dopants of N, P, Al and B during thermal oxidation of SiC films at 1200°C in dry O_2. Experimental segregation coefficients and interfacial concentration ratios were determined. Secondary ion mass spectrometry revealed that B and Al depleted from the SiC into the growing oxide while N and P were found to pile up in the SiC as a result of the loss of the SiC to the oxide formation. Aluminum is now used almost universally as the p-type dopant in SiC. The electrical properties of oxides thermally grown on n-type SiC normally have reasonably favorable characteristics of high breakdown voltage and low leakage currents. However, the reverse is true for thermally grown oxides on p-type SiC, as shown by Baliga and his students at NCSU. It is believed that at least two of the causes of the poor performance on a p-type material are the existence of the Al in the oxide and at the oxide/SiC interface and the dangling oxygen bonds which this species creates in the oxide as a result of a difference in oxidation state (+3) compared to that of Si (+4) and the existence of C at the SiC/insulator interface. Methods of effectively cleaning SiC surfaces prior to oxidation to deposit and grow oxides on p-type material under UHV conditions and determine the effect of Al redistribution and C concentrations at the interface on the properties of the oxide must be determined. In addition,

the effect of existing line and planar defects in the SiC epi-layer on the properties of the thermally grown and deposited oxide must be ascertained.

The research conducted in this reporting period and described in the following sections has been concerned with (1) design of a new CVD SiC system for the deposition of 6H- and 4H-SiC films, (2) studies of *ex situ* cleaning of various SiC surfaces in a variety of acids and bases, (3) design of a new, UHV compatible and integrated system of *in situ* cleaning, oxidation and oxide deposition on SiC, (4) the design of a mask set to fabricate metal oxide-semiconductor gated diodes as a test of the interface electrical properties between insulators and SiC, (5) measurement of diffusion lengths and calculations of carrier lifetimes of holes in 6H- and 4H-SiC, and (6) deposition, annealing and electrical characterization of Ni, NiAl and Au contacts to p-type SiC. The following individual sections detail the procedures, results, discussions of these results, conclusions and plans for future research. Each subsection is self-contained with its own figures, tables and references.

References

1. M. Bhatnagar, Ph. D. Thesis, North Carolina State University, 1994.
2. D. Alok, B. J. Baliga and P. K. McLarty, IEDM Technical Digest, IEDM 1993, 691 (1993).
3. R. C. A. Harris and R. L. Call in *Silicon Carbide–1973*, R. C. Marshall, J. W. Faust and C. E. Ryan, Eds. University of South Carolina Press, Columbia, S. C., 1974, pp. 534.
4. Suzuki, *et al.*, Jap. Journ. Appl. Phys. **21**, 579 (1982).
5. B. E. Deal and A. S. Grove, J. Appl. Phys. **36**, 3770 (1965).
6. J. W. Palmour, R. F. Davis, H. S. Kong, S. F. Corcoran and D. P. Griffis, J. Electrochem. Soc. **136**, 502 (1989).

II. Defects and Impurities in 4H- and 6H-SiC Homoepitaxial Layers: Identification, Origin, Effect on Properties of Ohmic Contacts and Insulating Layers and Reduction

A. Introduction

A silicon carbide system has been designed and the building process begun in order to grow silicon carbide thin films of high quality. Currently, the necessary components for the proposed system are being obtained. The design is modified as suggestions are received for optimizing the process.

B. Experimental Procedure

The system design (see Figs. 1 and 2) is comprised of a six-way cross, serving as a loadlock from which two separate chambers are attached. To one side of this loadlock is a growth chamber. To another side, perpendicular to the axis of the loadlock and growth chamber, is another chamber where RHEED analysis will be performed. The sample will be transferred to and from the various chambers on a SiC-coated graphite susceptor platform. The transfer mechanism consists of a platform which is moved from chamber to chamber by means of a manipulator rod which is screwed to the side of the susceptor.

The growth chamber consists of a rotating module to which the susceptor is placed. Growth will occur on the sample in an upside-down position with gases flowing upward while the susceptor is being rotated. The susceptor is attached to the rotating rod assembly from the groove into which the susceptor slides when transfer of the sample takes place. Once the sample is transferred to the rotating rod, the rod is brought down to the quartz portion of the sample located below the area where the sample was transferred into the growth chamber. Here, the sample is heated by an RF coil and gases are introduced from the bottom of the reactor. Growth temperature will be monitored by means of a standing pyrometer mounted outside the quartz chamber and aimed at the sample. Growth processes, such as gas flow rate and pressure, will be monitored by electronic components. Gas flow will be controlled by mass flow controllers and pressure by capacitance manometers.

The RHEED (Reflection high-energy electron diffraction) chamber, attached on another side of the loadlock chamber, will be attached to monitor film crystallinity, crystal structure and the formation of new surfaces. Since the growth of high-quality crystalline SiC films is being attempted, a RHEED chamber, attached to a nominal high vacuum to prevent direct exposure to atmosphere after growth, will be useful to characterize the film.

The SiC growth process will consist of introducing SiH_4 and C_2H_4 as the reactive components carried by a H_2 carrier. Nominal flow values will be on the order of 1 to 10 sccm for each. Carrier flows of H_2 will be on the order of 3 liters per minute. Other gases which will

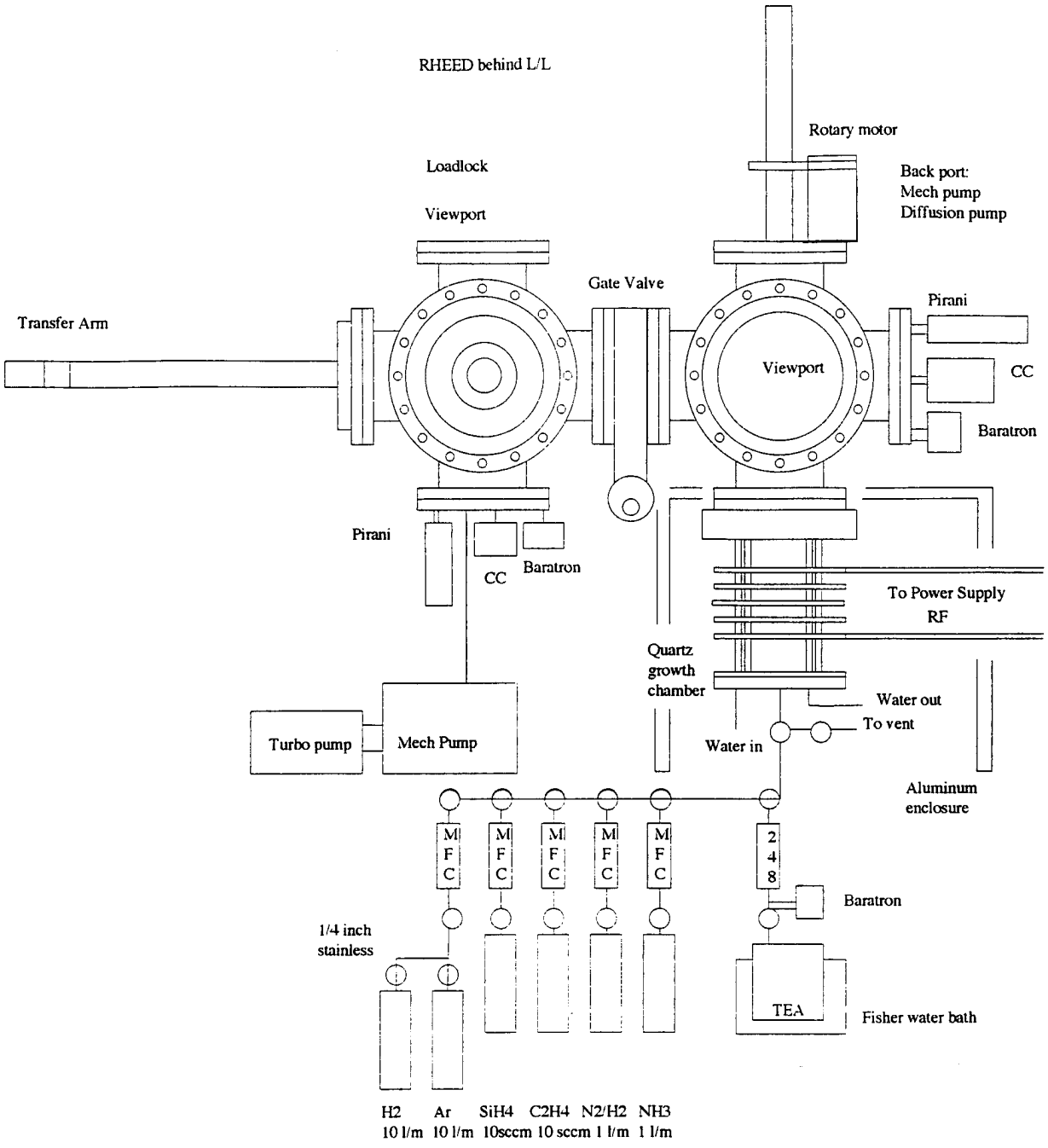

Figure 1. Schematic of SiC system.

be included on the system will be NH_3 and an N_2/H_2 mixture, for doping, and Ar. Also used for doping, TEA will be kept at constant temperature by a heater bath.

C. Results

To date, the design has been developed where sample transfer, growth, and RHEED analysis have been determined. Components are currently being ordered, see Table I.

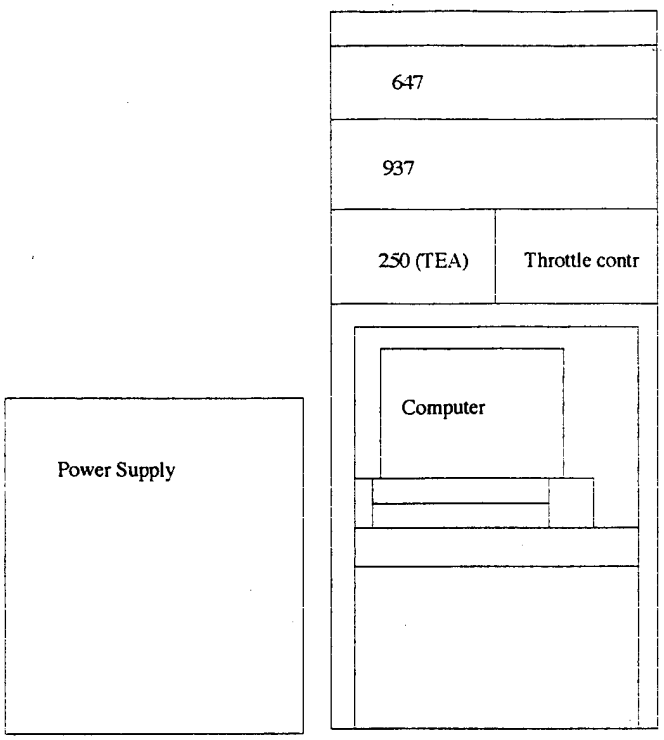

Figure 2. Schematic showing gauge system, 8-channel MFC controller, throttle controller, etc.

Table I. List of Components Ordered for SiC System

Vendor	Component
MKS	(2) 1000 Torr Baratrons (2) 10 Torr Baratrons 937 gauge system (2) 660 single channel gauges 640 integral pressure controller (2) cold cathode gauges throttle valve throttle valve controller 647 8-channel MFC controller various cables
Unit	(6) metal sealed MFC's
Cross	100 ft stainless steel tubing
Air Products	50g TEA, adduct grade
Fisher	(1) heating/cooling bath for TEA
Huntington	(2) 6-way crosses
Varian	(1) V-70 turbo pump

D. Discussion

The proposed design was developed with many sources of input. A number of constraints determined the design configuration and materials used in the system.

One of the main concerns was the high operating temperature of the growth chamber. Since temperatures around 1600-1700°C were going to be used to grow SiC thin films, it was determined that quartz would be the best material for the growth portion of the chamber. Once this was determined, a design had to be developed to cool the chamber. A double-walled quartz vessel, water cooled around the perimeter, was determined to be the optimum mode of cooling. Given the problems with achieving low pressures encountered in the past with the metal-to-quartz interface, it was determined that a metal-to-quartz fused sealed cylinder, available commercially, was the best way to insure that leaks could be minimized. With the assistance of Jim Futrell, an expert in quartz and glass design at the Microelectronics Center of North Carolina (MCNC), it was determined that such a vessel could be modified to accommodate water cooling.

Another concern was the transfer mechanism of the susceptor and the placement of samples on the susceptor surface. It was decided that small silicon carbide screws would be the most flexible for our purposes to accommodate various-sized samples. For the transfer mechanism, a simple tongue-in-groove assembly, moved between chambers by means of a transfer arm which would screw into the side of the susceptor, was deemed simple and most practical.

E. Future Research Plans and Goals

A design to deposit SiC thin films has been developed. Components are being ordered at this time. Vendors are still currently being consulted to determine the availability and compatibility of items for the proposed system. Further details of the design will be worked out in the coming months.

III. *Ex Situ* Cleaning Techniques for 6H-SiC Surfaces

A. Introduction

Silicon carbide (SiC) is a wide bandgap, compound semiconductor which has considerable potential in numerous electronic device applications involving high-power, high-speed, and high temperatures. The consideration of SiC as the semiconductor for these applications is based on the outstanding materials properties that it exhibits in demanding conditions including: high temperature stability (T_m=2800°C, under 30 atm Si), excellent oxidation resistance to 1000°C, high thermal conductivity, good radiation hardness and excellent thermal shock resistance [1]. Due to moderately close lattice matching and electrical conductivity, SiC has also become important as a heteroepitaxial substrate for III-V nitride compounds and alloys ($\Delta a/a_o$ SiC/AlN = 0.9%, SiC/GaN = 3.5%) which are the current materials of choice for yellow-blue-UV optoelectronic devices. The wide bandgap of the nitrides and their high saturated electron drift velocities at high fields also make these materials candidates for high-power and high-frequency microelectronics devices [2]. The development of SiC into the semiconductor/substrate of choice for these applications has been hampered by defects (i.e. micro-pipes, inversion domain boundaries (IDB's), double position boundaries (DPB's), stacking faults and twins) formed during bulk crystal growth and homo/heteroepitaxy. Though the solution to the further reduction of many of these defects in both SiC and III-N's may lie in other materials issues, a continued reduction in defect densities (dislocations, stacking faults, IDB's, etc.) may eventually depend on a better understanding and development of SiC surface preparation and cleaning. In fact, a clear relation between surface cleaning/preparation and device performance has already been demonstrated in Si and GaAs semiconductor technologies [3, 4].

In silicon homoepitaxy, improper removal of surface contamination and oxides prior to epitaxy has been clearly shown to result in an increase in the density of line and planar defects (i.e. dislocations, stacking faults, and twins), from $<10^4/cm^2$ to $>10^{10}/cm^2$ [5-10]. More importantly from an economic point of view, increased epitaxial defect densities have been shown to result in a significant drop in device yield [5,6]. Surface cleaning has also been found important in the formation of metal contacts (Ohmic or Schottky). Improper removal of surface oxides prior to metal deposition has been shown to result in higher contact resistances, thermal instability, and lack of parameter uniformity [11-15]. Further, the Schottky barrier height in metal contacts can also be influenced by the existence and density of surface/interface states in the band gap of a semiconductor. These interface states can pin the position of the Fermi level in the semiconductor and determine the Schottky barrier height. As most surface/interface states are related to surface dangling bonds, surface preparation/cleaning can be used to passivate these dangling bonds and control the existence and density of surface/interface states in metal

contacts [15-18]. In MIS devices, control of interface states densities is also important as they can produce swings in threshold voltages. Drift in MIS parameters has also been linked to the presence of alkali ions at the interface and this in part can also be controlled by surface cleaning prior to insulator deposition [19,20]. In summary, it has been demonstrated in other materials systems that surface cleaning/preparation can permeate all aspects of semiconductor processing, adversely affecting: epitaxy, contacts (Ohmic or Schottky), and insulator performance. For these reasons, it should not be surprising that 50% of all yield losses in silicon IC fabrication are attributed to micro contamination.

The intent of this study, therefore, has been to examine *ex situ* cleaning techniques for SiC surfaces which have been found useful in Si and GaAs technologies. However, the focus of this study has been to not only find techniques which obtain "clean" SiC surfaces but to also obtain a more fundamental understanding of the chemistry which takes place at SiC surfaces. In this study, "clean" will be taken to mean complete removal (within the detection limits of the analytical techniques employed) of the two principle contaminants on SiC surfaces, namely, oxygen and non-carbidic carbon. Other contaminants such as fluorine, alkali ions, etc. can also be present on SiC surfaces which can equally create defects and ruin SiC devices. However, these contaminants have not yet been addressed in this study. The two *ex situ* cleaning techniques addressed so far in this study include wet chemical oxide removal using HF based solutions and/or UV/ozone oxidation for non-carbidic carbon removal. Both of these techniques have been found very useful in Si technology.

For silicon, HF etches have been found very beneficial as it not only etches away any silicon oxide at the surface, but passivates all of the silicon dangling bonds at the surface with hydrogen. The hydrogen termination inhibits re-oxidation of the silicon surface on removal from the HF solution and produces a very hydrophobic surface [21,22]. UV/Ozone oxidation treatments have been found very useful in Si and GaAs cleaning for mainly removing carbon contamination from these surfaces. In this technique, Si or GaAs samples are exposed to UV radiation from a Hg lamp which emits light at 253.7 nm (90%) and 184.9 nm (5%). The 253.7 nm light is absorbed by most hydrocarbons and will excite C-C and C-H bonds. The 253.7 nm line is also absorbed by ozone. The 185 nm light is absorbed by O_2 and creates O_3 (Ozone) [23,24]. The effect is that adventitious carbon is excited, oxidized, and removed from the Si or GaAs surface. The oxide formed on the surface by the O_3 exposure can then be removed by either wet chemicals or by *in situ* thermal desorption.

B. Experimental Procedure

Substrates. The samples used in these experiments were 1" diameter, n-type (N_d=1×10^{18}), $(0001)_{Si}$ and $(0001)_C$ 6H-SiC wafers obtained from Cree Research (Durham, NC). For the (11-20) and (10-10) orientations, roughly 7 mm × 7 mm fragments of n-type wafers, also from

Cree, were used. On axis and off axis "vicinal" (4° off toward (11-20)) $(0001)_{Si}$ 6H-SiC wafers were also investigated. All wafers came with an ≈ one micron epi layer (N_d=5×10^{17}) and an ≈ 500-1000Å thermal oxide both grown by Cree. The use of thermal oxides was based on work by L. Porter who found this oxide layer was instrumental in generating a stoichiometric SiC surface after removal with HF. For these studies, the thermal oxide was removed using a 10% HF solution. Further cleaning of this surface was then examined by immersion in other acid/base solutions or by re-oxidizing the SiC surface using a UV/ozone treatment followed by wet chemical treatment. UV/ozone treatments described in this study employed UV/Ozone box which positioned a high intensity Hg lamp in close proximity to the SiC wafer and has been described elsewhere [23,24]. The wet chemistries examined included 10% HF, 10% Buffered HF (7:1 NH_4F:HF), 40% NH_4F, HCl:HF and NH_3OH:HF solutions, HNO_3, H_2SO_4, Acetic, and Lactic acid. Except where noted, after all wet chemical cleans the samples were rinsed in DI water (18MOhm) and blown dry with N_2 (UHP). All wet chemicals were of CMOS grade purity (J. T. Baker). Surfaces prepared in the above manner were then subsequently mounted to a molybdenum sample holder for analysis by AES, XPS, EELS, and LEED.

Analytical Procedure. All of the surface analysis described in this paper was conducted in a unique ultra high vacuum (UHV) system which integrates several completely independent UHV units via a 36 ft. long transfer line (see Fig. 1). The details of this integrated system have been given in previous ONR reports [25]. Briefly, it currently incorporates a remote H-plasma/CVD system, an ASTeX diamond deposition system, *in situ* Raman Spectroscopy, a VSW angle resolved ultra-violet photoelectron spectroscopy system (AR-UPS), an e-beam Si and Ge MBE, an analysis system including a Perkin Elmer Auger electron spectrometer and Princeton Instruments LEED (low energy electron diffraction) optics, a five source (Al, Au, Cu, Ti, Zr) e-beam metal deposition system, a III-V nitride GSMBE, and an X-ray photoelectron spectroscopy (XPS) system.

XPS System. X-ray photoelectron spectroscopy experiments were performed in a stainless steel UHV chamber equipped with a dual anode (Mg/Al) x-ray source (VG XR3E2) and a 100 mm hemispherical electron energy analyzer (VG CLAM II). The base pressure in this system was 1×10^{-10} Torr and was pumped by 220 l/s ion pump (Varian). All XPS spectrums reported here were taken using Al Kα radiation (hυ=1486.6 eV) with 12 kV and 25 mA emission current. XPS analysis required less than 1 hour during which the pressure never rose above 9×10^{-10} Torr. Calibration of the binding energy scale for all scans was achieved by periodically taking scans of the Au $4f_{7/2}$ and Cu $2p_{3/2}$ peaks from standards and correcting for the discrepancies in the measured and known values of these two peaks (83.98 and 932.67 eV, respectively). Curve fitting of most data was performed using the software package

GRAMS 386. A combination Gaussian-Lorentzian curve shape with a linear background was found to best represent the data.

AES/LEED/EELS. The Auger electron spectrometer (Perkin Elmer 10-155 CMA) and the low energy electron diffraction optics (Princeton Instruments) were mounted on a six-way cross off the transfer line and pumped through the transfer line. In AES analysis, a 3 keV, 1 mA beam was used and the Auger spectrum was collected in the undifferentiated mode and then numerically differentiated. In EELS and LEED, an 80 eV, 1 mA beam was used. EELS spectrums were also collected in the undifferentiated mode.

C. Results

$(0001)_{Si}$ - Wet Chemical. After removal of the thermal oxide with a 10% HF solution, AES, XPS, and EELS of all the 6H-SiC orientations (i.e. $(000\text{-}1)_C$, $(0001)_{Si}$, and (11-20) and (10-10)) all showed the surfaces to contain various amounts of oxygen and non-carbidic carbon. As it was difficult with these spectroscopies to distinguish major differences between the various orientations after thermal oxide removal, data from an off axis, vicinal $(0001)_{Si}$ 6H-SiC surface will be presented first to represent the general trends observed. The finer details of *ex situ* cleaning for the other orientations will then be presented.

Figure 1a shows an XPS spectrum of the O 1s peak from a vicinal $(0001)_{Si}$ 6H-SiC wafer after removal of the thermal oxide by dipping in 10% HF. As can be clearly seen, there is still a significant amount of oxygen on the SiC surface even though a chemically shifted Si 2p oxidation peak was not was seen from the this surface. For comparison purposes, Fig. 1b shows the O 1s from a vicinal Si (111) wafer after dipping in 10% HF. There is a striking difference in the amount of oxygen left on the two surfaces after HF dipping. This complements the observation that the Si surface was hydrophobic after HF dipping and the SiC surface hydrophilic. Specifically, the Si wafer could be pulled dry from the HF solution whereas when withdrawing a SiC wafer from HF, the HF solution still wetted the SiC surface. After HF dipping, the O 1s position occurs at 533.1 eV for the SiC surface and 531.5-531.8 eV for the Si (111) wafer. For further comparison, the O 1s from a CVD diamond film on silicon was measured and found at 532.0-532.6 eV. The reason for these differences will be discussed later. Small amounts of fluorine on the SiC surface after HF dipping were also detected by XPS. The amount of fluorine detected varied from day to day and appeared to be dependent on the DI rinsing time. (1×1) LEED patterns were easily obtained from both on and off axis $(0001)_{Si}$ SiC surfaces after dipping in 10% HF. The LEED patterns were intense with a diffuse background. The LEED spots, however, were large and fuzzy and could not be focused into dots. This is presumably due to the significant disorder produced in the surface after oxide removal with HF. All of the above observations were also made for on axis $(0001)_{Si}$ 6H-SiC.

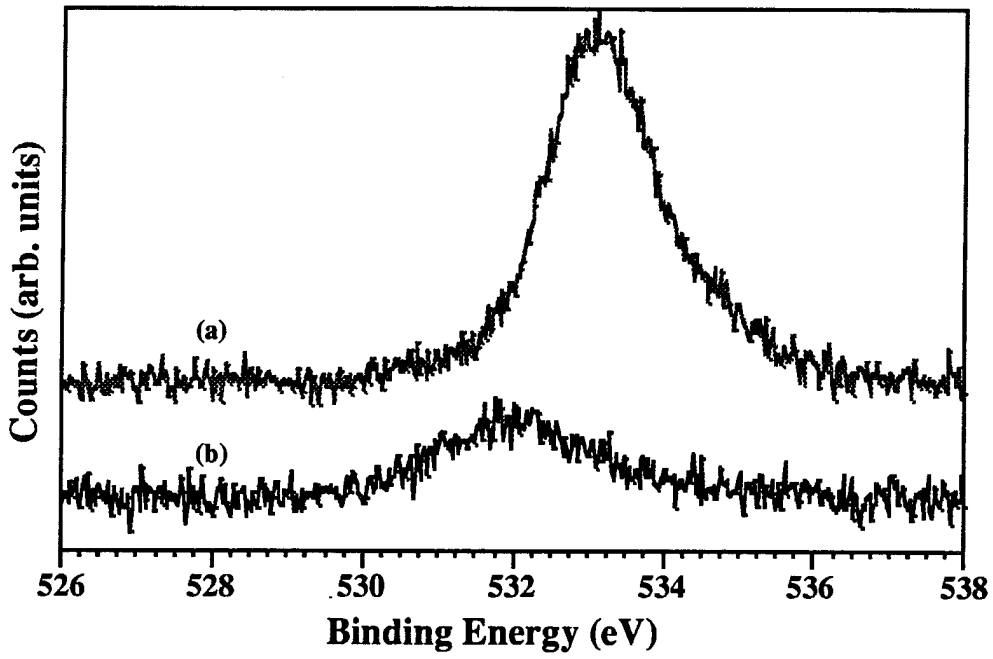

Figure 1. XPS of O 1s from (a) vicinal $(0001)_{Si}$ 6H-SiC and (b) off axis Si (111) after dipping in 10% HF 5 min., DI rinse, and N_2 blow dry.

To illustrate that an HF dip does remove silicon oxides from SiC surfaces (which may form due to ambient exposure), a vicinal $(0001)_{Si}$ 6H-SiC wafer was intentionally re-oxidized by annealing in a unbaked GSMBE. Figure 2a shows an XPS spectrum of the Si 2p peak from the re-oxidized vicinal $(0001)_{Si}$ 6H-SiC wafer. Two peaks are clearly distinguished. The most intense peak at 101.5 eV (FWHM=1.4 eV) is characteristic of Si-C bonding and is from the SiC wafer. The less intense peak/shoulder at 103.2 eV (FWHM=2.6 eV) is characteristic of silicon in a +4 oxidation state (i.e. O-Si-O bonding) and is from a silicon oxide layer which has formed on the SiC wafer. The width of the 103.2 eV peak is 2.6 eV and is probably a mixture of +2, +3, and +4 oxidation states (i.e. Si-O, O-Si-O, and Si-OH). Figure 3a shows an XPS spectrum of the C 1s peak from the same SiC wafer. This spectrum also shows two peaks. The narrow peak at 283.6 eV (FWHM=1.1 eV) is indicative of C-Si bonding, whereas the broad peak at 285.5 eV (FWHM=1.9 eV) is probably a mixture of C-H, C-O, and C-C bonding presumably from dust, organic particulates, bacteria etc. The O 1s core level for this surface was located at 531.1 eV which is indicative of silicon dioxide. LEED patterns were not obtained from this surface. It should be noted that SiC wafers exposed to ambient at room temperature for several days to months after dipping in HF do not exhibit this level of oxidation.

Dipping the above vicinal wafer in 10% HF was found to remove the silicon oxide layer and some of the hydrocarbon contamination from the SiC surface. Figure 2b shows an XPS

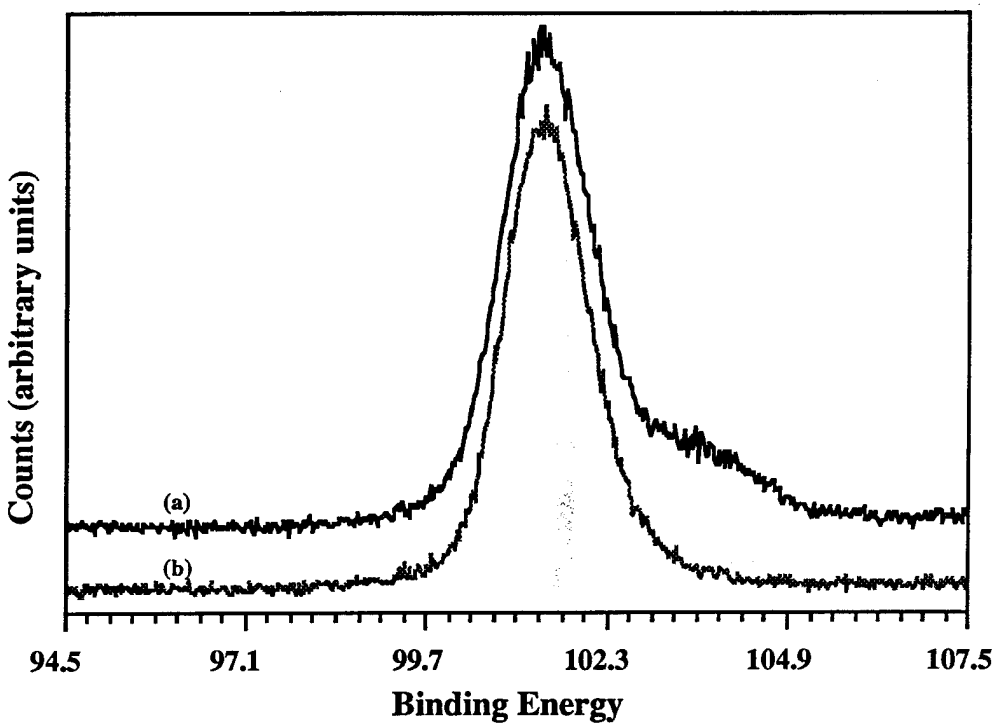

Figure 2. XPS of Si 2p from vicinal $(0001)_{Si}$ 6H-SiC surface: (a) after oxidation in GSMBE during bakeout and (b) after dipping in 10% HF for 5 min., DI rinse, and N_2 blow dry.

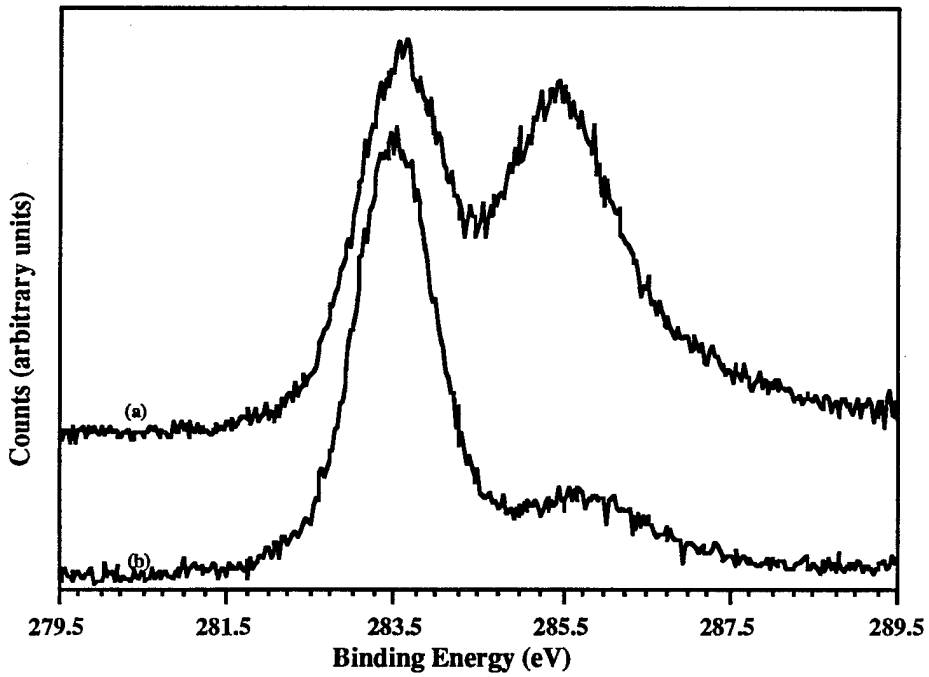

Figure 3. XPS of C 1s from vicinal $(0001)_{Si}$ 6H-SiC surface: (a) after oxidation in GSMBE during bakeout and (b) after dipping in 10% HF for 5 min., DI rinse, and N_2 blow dry.

spectrum of the Si 2p peak from the same SiC wafer immediately after dipping in 10% HF. In comparison with Fig. 2a, there is no peak at 103.2 eV indicating removal of the silicon oxide layer from the SiC surface. As seen in the XPS spectrum of the C 1s (Fig. 3b), dipping in HF also reduces (though incomplete) the level of noncarbidic contamination on the SiC surface. The presence of non carbidic carbon after HF dipping is also detected in EELS via a π-π^* loss peak typically at 2-3 eV labeled "non carbidic" carbon in Fig. 4a. In EELS, surfaces are exposed to low energy electrons (E_p typically 100 eV) and the energy distribution of the back scattered electrons are measured. Most of the electrons are elastically scattered from the surface (i.e. no energy loss) and return to the detector with energy equal to the beam energy. A smaller number ($\approx$ 0.1-1%) of the electrons are inelastically scattered due to collisions and excitation of plasma frequencies in the semiconductor conduction band. As the elastic peak is so large with respect to the rest of the loss features, it is usually truncated in order to more easily display the pertinent loss data. The broad features ranging from 10 to 25 eV are due to excitation of both SiC surface and bulk plasmons (16 and 23 eV, respectively). The loss peak at 2-3 eV is always directly correlated with a strong C 1s XPS peak at 285-286 eV and is not thought to be due to graphite which would have a loss peak at 6 eV.

In order to find a wet chemistry which produces a more hydrophobic SiC surface, several $(0001)_{Si}$ 6H-SiC wafers were dipped in various acids and bases and the wetting characteristics

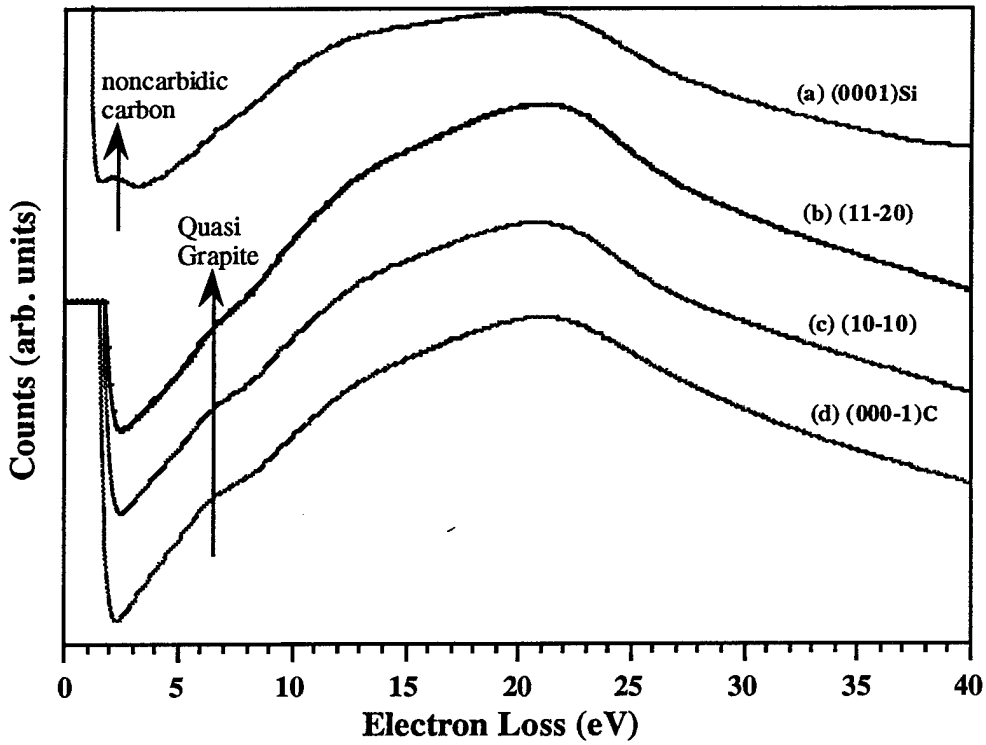

Figure 4. EELS of different 6H-SiC orientations after dipping in 10% HF 5 min., DI rinse, and N_2 blow dry: (a) $(0001)_{Si}$, (b) (11-20), (c) (10-10), (d) $(000\text{-}1)_C$.

of these surfaces in de-ionized water were monitored visually. The acids and bases examined included: HF, NH_4F, NH_3OH, HCl, HNO_3, H_2O_2, H_2SO_4, Acetic, and Lactic acid. For comparison purposes Si (111) and (100) wafers were also dipped simultaneously in each acid with the SiC wafer. All wafers (Si or SiC) were initially dipped in 10% HF to remove any native oxides from the surfaces before dipping in the acid of interest. For Si, the surfaces remained hydrophobic when dipped in NH_3OH, HCl, or H_2O_2. Dipping the Si wafers in HNO_3 or H_2SO_4 removed the hydrophobic nature of the surface. Dipping Si in the organic acids resulted in a strongly adhering thin film of the acid to the silicon surface which could be rinsed off in DI leaving a hydrophobic Si surface. For SiC, all acids and bases wetted the surface and nothing was found which produced a hydrophobic SiC surface. HF solutions with various pH's adjusted from strongly acidic, neutral, and to strongly basic using HCl, NH_4F, and NH_3OH, respectively, were also examined as they have been reported to produce better hydrogen termination of Si surfaces. In these experiments the dipping times were held constant at 10 min. and no changes in the wetting characteristics of the $(0001)_{Si}$ SiC surface in HF solutions with different pH's were found. In one experiment, the dipping time was varied from 5 min. to 1 hr. and once again no differences were found. Additionally, neither XPS nor AES indicated a significant change (within AES and XPS experimental accuracy) in the amount of surface oxygen on $(0001)_{Si}$ SiC wafers after dipping in HF solutions of various pH. No differences were observed between on axis and vicinal surfaces, as well.

$(0001)_{Si}$ UV/Ozone. Figure 5a shows an XPS spectrum of the C 1s peak from a $(0001)_{Si}$ 6H-SiC surface prior to exposure to UV/Ozone oxidation. As in Fig. 3, two C 1s peaks are clearly distinguished at 285.7 eV and 283.5 eV which are due to non-carbidic carbon and carbidic carbon, respectively. This surface had been previously dipped in 10% HF to remove any silicon oxide from the SiC surface. Figure 5b shows the C 1s from this surface after exposure to UV/Ozone for 5 hours. As can be seen, there are still two C 1s peaks. However, the non-carbidic carbon peak has shifted from 285.7 eV to 285.2 eV whereas the carbidic carbon peak remains unshifted at 283.5 eV. Further as shown in Fig. 6, a chemically shifted Si 2p peak at $\approx$ 103 eV is also detected after the UV/ozone exposure indicating the formation of some silicon oxide. Unfortunately, longer exposures (18 hours) were not found to produce any further changes in the amount or position of the non-carbidic C 1s peak.

$(000\text{-}1)_C$, (11-20), and (10-10). Figure 7(a-d) shows a series of AES spectrums taken from surfaces of the four primary orientations of 6H-SiC: $(0001)_{Si}$, $(000\text{-}1)_C$, (11-20), and (10-10). Each spectrum is normalized to make the carbon KLL Auger peak to peak height (pph) the same. As shown in Fig. 7, the oxygen levels after HF dipping for the $(000\text{-}1)_C$, (11-20), and (10-10) surfaces were not found to differ appreciably from those found for the vicinal $(0001)_{Si}$ surface. Table I lists the Si/C, O/Si, and O/C pph AES ratios (uncorrected for differences in sensitivity) calculated for each surface.

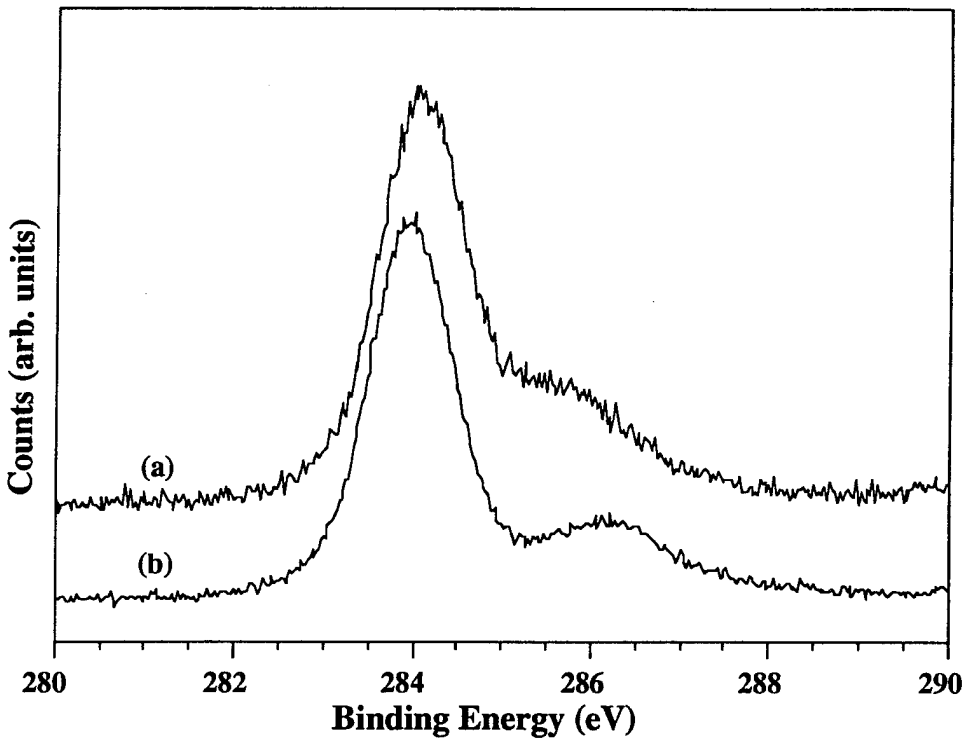

Figure 5. XPS of C 1s from $(0001)_{Si}$ 6H-SiC: (a) before UV/Ozone oxidation and (b) after 5 hours of UV/Ozone oxidation.

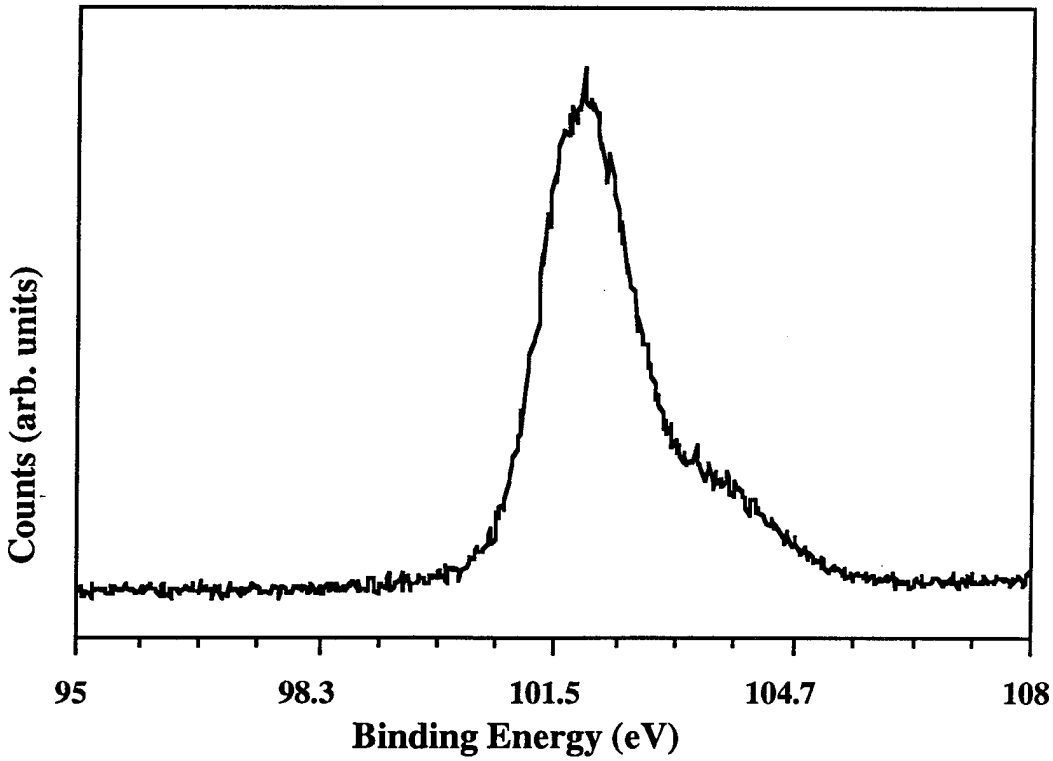

Figure 6. XPS of Si 2p from $(0001)_{Si}$ 6H-SiC after UV/Ozone oxidation for 5 hr.

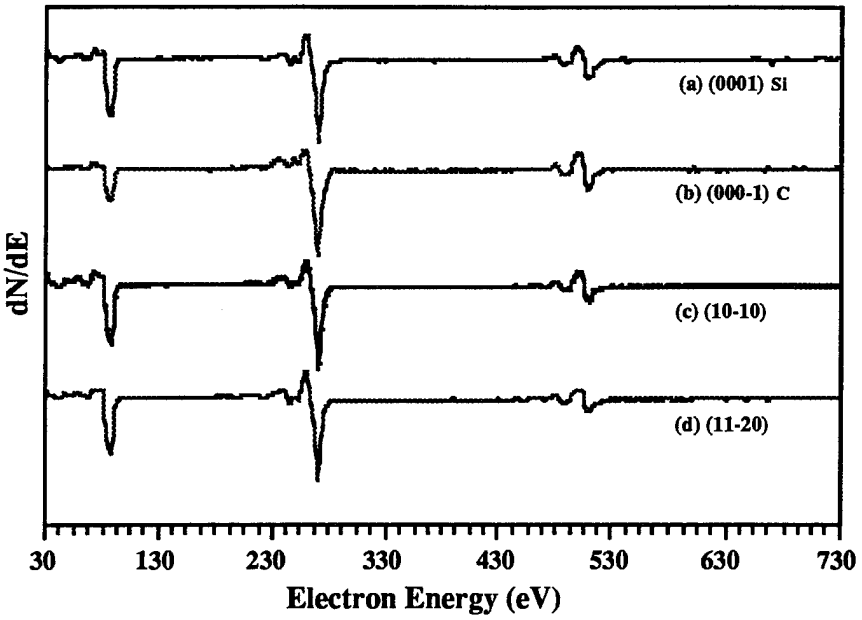

Figure 7. AES spectrum from 6H-SiC surfaces of different orientations after dipping in 10% HF 5 min., DI rinse, and N_2 blow dry: (a) $(0001)_{Si}$, (b) $(000\text{-}1)_C$, (c) (10-10), and (d) (11-120).

Table I. Peak to Peak Height (pph) Ratios for Various 6H-SiC Surfaces

	$(0001)_{Si}$	$(000\text{-}1)_C$	(11-20)	(10-10)
Si/C	0.60	0.34	0.61	0.65
O/Si	0.52	0.99	0.37	0.43
O/C	0.31	0.34	0.23	0.28

Table I shows the O/C ratio for all the different orientations of 6H SiC surfaces to be centered around 0.3. Given that two of these surfaces are polar and the others non polar, it surprising that they would exhibit this similarity. Further, the Si/C ratio for the $(0001)_{Si}$, (11-20), and (10-10) surfaces are all centered around 0.6 which is also surprising in that ideally the $(0001)_{Si}$ surface would be terminated exclusively with Si, whereas the (10-10) and (11-20) are nonpolar surfaces ideally with equal numbers of carbon and silicon atoms at the outermost surface. The $(000\text{-}1)_C$ surface, however, shows a Si/C ratio half that found for the $(0001)_{Si}$ which is expected based on the differences in polarity for these two surfaces. The O/Si ratio for the $(000\text{-}1)_C$ surface was found to be twice that for the other orientations indicating the possibility that a significant amount of oxygen is actually bonded to carbon at SiC surfaces.

Like the $(0001)_{Si}$ face, EELS of the $(000\text{-}1)_C$ surface shows a non carbidic π-π^* carbon loss peak which is interestingly shifted to 4-5 eV. This is much closer to where one would expect to find a loss peak for graphite (see Fig. 4(d)). EELS of the $(000\text{-}1)_C$ surface also shows a more drastic drop off at 10-15 eV than the $(0001)_{Si}$ surface. XPS of the $(000\text{-}1)_C$ surface like the $(0001)_{Si}$ surface shows two C 1s peaks but the values are shifted to lower binding energies of 282.8 eV and 285.0 eV (FWHM=1.1 and 2.5 eV respectively). The non-carbidic C 1s peak at 285.0 eV (like the EELS peak) is close to the value of 284.5 eV which has been reported for graphite. This result indicates that the non carbidic carbon left on the $(000\text{-}1)_C$ 6H-SiC surface after HF dipping is closer in similarity with graphite than the noncarbidic carbon on the $(0001)_{Si}$ surface. XPS of the Si 2p and O 1s from the $(000\text{-}1)_C$ 6H-SiC surface after HF dipping are also shifted to lower binding energies with the Si 2p at 100.7 eV (FWHM=1.3 eV) and the O 1s at 532.5 eV (FWHM=2.3 eV). The lower core level values for the $(000\text{-}1)_C$ face could be due to differences in doping, wafer growth and processing, step density, band bending etc., but the position of the O 1s core level at 532.5 eV is intriguingly close to the previously mentioned value from a CVD diamond film.

Surprisingly, EELS spectrums of the (11-20) and (10-10) surfaces are identical to those taken from the $(000\text{-}1)_C$ surfaces which contrasts with the AES results which showed similarities between the $(0001)_{Si}$ and the (11-20) and (10-10) surfaces (see Fig. 4(b,c)). XPS of the (11-20) and (10-10) surfaces gave results intermediary between those found for the $(0001)_{Si}$ and $(000\text{-}1)_C$ surfaces. The values obtained for the (11-20) Si 2p, C 1s, and O 1s are respectively: 101.6 eV, 283.5 and 284.7 eV, and 532.5 eV. The Si and C core levels are similar to those for the $(0001)_{Si}$ surface. However, the non carbidic C 1s and O 1s core levels are closer to those found for the $(0001)_C$ surface.

LEED patterns were easily obtained from the $(000\text{-}1)_C$, (11-20), and (10-10) surfaces after HF dipping. The $(000\text{-}1)_C$ surface exhibited a (1×1) pattern similar to that observed for the $(0001)_{Si}$ surface after HF dipping. The (11-20) and (10-10) surfaces revealed rows of dots which have been tentatively assigned to (1×1) patterns.

The wetting characteristics of the $(000\text{-}1)_C$, (11-20), and (10-10) 6H-SiC surface orientations in various acids and bases were also examined. In all cases, these surfaces exhibited wetting characteristics similar to those found for $(0001)_{Si}$. The only exception found was one particular $(000\text{-}1)_C$ wafer which was found to pull dry from HF. AES and XPS analysis revealed this wafer to contain an uncharacteristically significant amount of nitrogen at the surface. Investigations are currently underway to locate the source of this nitrogen.

D. Discussion

$(0001)_{Si}$ 6H-SiC-Wet Chemistry. The AES and XPS spectrums obtained in this study from $(0001)_{Si}$ 6H-SiC wafers after HF dipping are similar to those published in previous

studies [26-29]. Unfortunately, none of these papers attempted to address the nature of the remaining oxide and to what the surface oxygen was bonded. Figure 1(a, b) illustrates that the amount of oxygen left on the SiC surface after HF dipping is much larger than that for a silicon surface of the same crystallographic orientation. The position of the O 1s in XPS for both of these surfaces is also different with the O 1s for SiC at 532.5-533.1 eV and the O 1s for Si at 531.5-531.8 eV. This is important as the 6H-SiC $(0001)_{Si}$ surface has been assumed by many to be similar to the Si (111) surface. Ignoring band bending effects and interpreting based strictly on chemical shifts, Table II would seem to indicate that after HF dipping the oxygen left on the SiC surface is predominantly silicon oxide while the oxygen left on Si is predominantly a hydroxide. This interpretation is difficult to accept based on the fact that HF is known to etch SiO_2 at a rate of 10000Å/sec. However, this conclusion could be in error as it ignores the possibility of carbon and oxygen bonding at the SiC surface. Even though the $(0001)_{Si}$ surface ideally is silicon terminated, perhaps the differences observed between the Si (111) and 6H-SiC $(0001)_{Si}$ surfaces lie in the possibility of oxygen termination of carbon atoms. Recent STM studies of 6H-SiC surfaces have shown that a significant number of steps exist with step

Table II. Observed Si 2p, C 1s, and O 1s Core Level Positions for Different Materials from XPS Handbook

Si 2p			
SiO_2	103.6 eV	Si	99-100 eV
SiO_2-alpha crist	103.3 eV	Si_3N_4	101.8 eV
SiO_2-apha quartz	103.6 eV	$Ph_3SiOSiPh_3$	101.3 eV
SiO_2-Vycor	103.5 eV		
C 1s			
Graphite	284.3-285.5 eV	$(C^*HCOH)_3$	284.8 eV
CO_2	291.9 eV		
$(CHC^*OH)_3$	286.6 eV		
$CaCO_3$	289.6 eV		
$Fe(CO)_5$	288.0 eV		
Benzene	284.7 eV		
$C_6H_5C^*H_3$	284.7 eV		
HCHO	287.7 eV		
O 1s			
Sapphire	531.0 eV	p-Benzoquinone	532.2 eV
Alpha-Al_2O_3	531.8 eV	Hydroquinone	533.5 eV
Gamma-Al_2O_3	530.9 eV	Methylsilicone Resin	532.7 eV
$Al(OH)_3$-Bayerite	531.4 eV	Phenylsilicone Resin	532.6 eV
$Al(OH)_3$-Gibbsite	531.5 eV	SiO_2	532.5-533.0 eV
AlOOH-Boehmite	531.5 eV	SiO_2, alpha quartz	533.2 eV
$Ph(CONH_2)$	532.2 eV	SiO_2, gel	532.8 eV

heights of 20-40Å where plenty carbon atoms are exposed at the surface. Additionally, surface studies of air exposed diamond have shown this surface to be oxidized, as well [30-32]. So it is reasonable to consider the possibility of both C-O and Si-O bonding at the SiC surface. In a separate study by the authors, XPS was used to examine an air exposed CVD diamond film (grown on Si). For this surface, the O 1s peak position was located at 532.6 eV as received and 532.0 eV after cleaning. This appears to rule out the possibility of carbon-oxygen bonding at the SiC surface. However, band bending is known to occur at both diamond and SiC surfaces due to the presence of surface states, and this can affect the position of the O 1s core level on both of these surfaces. Table II also shows that the O 1s ranges from 532-533 eV for both compounds containing C-O and Si-O bonds. Thus, analysis of the O 1s peak position therefore can not confirm or exclude the possibility of carbon-oxygen bonding at the SiC surface. Therefore, it may be better to look for chemically shifted components on the Si 2p and C 1s core levels.

Figure 2b clearly shows that after HF dipping, a chemically shifted Si 2p peak at 103.2 eV does not exist and this excludes the presence of a thin silicon dioxide layer. However, this does not exclude the presence of lower silicon oxidation states which would be chemically shifted by lesser amounts. Hollinger and Himpsel [33] using SXPS were able to distinguish four different chemically shifted oxidation states of silicon after low pressure oxidation which were: $Si^{(+1)}$ - 1.0 eV, $Si^{(+2)}$ - 1.8 eV, $Si^{(+3)}$ - 2.7 eV, and $Si^{(+4)}$ - 3.5 eV. As the chemical shift for Si to SiC ranges from 1.0 to 1.8 eV, identification of silicon atoms in lower oxidation states at the SiC surface is complicated due to overlap with the main Si-C Si 2p peak. Further complication arises from the asymmetric peak shape of the Si 2p which is actually two peaks (Si $2p_{3/2,1/2}$ doublet) which are unresolvable with our XPS instrument. The combined resolution and overlap problems, preclude the identification of Si-O and Si-OH bonding through the Si 2p photoelectron peak. For the C 1s these problems do not exist. Figure 3b, shows the presence of both a broad (1.9 eV) and a narrow (1.1 eV) C 1s peak at 283.8 and 285.5 eV respectively. The lower binding energy C 1s peak is due to C-Si bonding and is from the SiC substrate. The higher binding energy peak is from carbon at the surface in a mixture of CH_2 (284.6 eV), C-O (286.3 eV), and some O-C=O (288.4 eV) bonding configurations [34-35]. Based on these values, it is tempting to assign all of the carbon in the 285.5 eV C 1s peak to being predominantly C-O. These results are also in good agreement with those of Miyauchi *et al.* who found that surface carbon remaining on Si (100) after dipping in 5% HF was composed predominantly of C-O bonding [35]. Using higher concentrations of HF (49%), they found the surface carbon to contain predominantly more O-C=O bonding where as low HF concentrations (0.05-0.5%) left surface carbon predominantly in CH_2 bonding. Unfortunately, this does not account for all the oxygen at the SiC surface.

An alternative explanation for the difference in surface oxygen coverage for HF dipped Si (111) and SiC $(0001)_{Si}$ surfaces could be an inability of HF to hydrogen terminate the SiC surface or an instability of the hydrogen termination produced. It has been well documented that for silicon, HF dipping removes the surface oxide and terminates the surface with hydrogen [21,22,33]. On removal from HF, the hydrogen passivation of the silicon surface prevents re-oxidation of the silicon surface by DI rinsing or exposure to air. This may not be true for SiC surfaces, though. Dipping in HF may not create a hydrogen passivated SiC surface or alternatively, the hydrogen passivation of the SiC surface could be weaker and more susceptible to oxidation in the HF solution or air. For diamond, HF has not been found to produce a hydrogen terminated surface [36]. A possible explanation for weaker hydrogen termination of $(0001)_{Si}$ SiC surfaces in HF may lie in the differences in the underlying bonding. Though both Si (111) and $(0001)_{Si}$ 6H-SiC surfaces are terminated with Si atoms with one dangling bond each, the underlying bonding of the silicon surface atoms for these two surfaces is completely different. Si atoms at the surface of Si (111) have three underlying Si-Si bonds whereas in $(0001)_{Si}$ SiC there are three underlying Si-C bonds. Since C is more electronegative than Si, most of the Si valence electrons in SiC will be drawn toward the underlying C atoms leaving less electrons at the SiC surface for silicon-hydrogen bonding than for silicon surfaces. This could make the Si-H bond in $(0001)_{Si}$ SiC surfaces weaker than those formed in Si (111) surfaces, thus making H termination more difficult to achieve with HF (a weak acid) and maintain on removal from HF and exposure to air. This line of reasoning is somewhat supported by the work of Didziulis *et al.* [37] who using SXPS and molecular orbital theory conducted a detailed analysis of the $(000\text{-}1)_C$ face of 6H-SiC. Their findings indicated that the highest occupied energy levels in SiC are mostly of C 2p character and that carbon atoms would be the preferred site for an electron withdrawing adsorbate. This implies that oxidation of the SiC surface is more likely to initiate at carbon sites than at silicon sites (which prefer electron donating adsorbates). Considering the equilibrium in aqueous solutions is usually a balance between H^+ and OH^- ions. Carbon sites would be preferred for H^+ adsorption and silicon sites would be preferred for OH^- adsorption. Since HF aggressively breaks Si-O bonds by the formation of SiF_6^{2-} (the overall reaction is $SiO_2 + 6HF = 2H^+ + SiF_6^{2-} + H_2O$), it would be expected that all Si-O species would be quickly removed as soon as they are generated [38,39]. This would eventually leave a carbon rich surface with lots of free carbon at the surface (assuming that HF doesn't remove this free carbon). The free surface carbon would be mostly of C-H and C-OH bonding. This is in fact exactly what is observed. Given that AES is more sensitive to silicon than carbon, the AES Si/C pph ratios in Table I clearly show that the SiC surface is carbon rich even though crystallography indicates that it should be silicon terminated. Further, XPS and EELS both show the presence of sizable

amounts of noncarbidic carbon at the surface which are much larger than what is typically observed for silicon.

Perhaps the ideal analytical technique for determining whether hydrogen termination of SiC surfaces is achieved with HF would be high resolution electron energy loss spectroscopy (HREELS). HREELS is ideally suited for answering this type of questions as it can detect C-O, Si-O, Si-OH, Si-H, C-H "molecular" vibrations at semiconductor surfaces. Unfortunately, the work of M. Dayan and Starke *et al.* [40,41] indicates that this technique is not suitable for studying SiC surfaces as excitation of Fuchs-Kliewer phonons interferes and dominates the EELS spectrum. Due to the overlap with the FK loss peaks, Starke *et al.* were not able to exclude or conclude the presence of Si-H bonding at the SiC surface. However, they were at least able to use HREELS to identify the presence of OH^- groups at the $(0001)_{Si}$ surface after HF dipping. This agrees well with the observed hydrophilic nature of the SiC surface after HF dipping.

Perhaps the strongest argument against the possibility of hydrogen termination of SiC surfaces by HF dipping is the simple observation that for 10% HF solutions SiC surfaces are still hydrophilic on removal from HF whereas Si wafers are hydrophobic. The nature of the termination of the $(0001)_{Si}$ 6H-SiC surface could depend on the chemistry of the HF solution. HF is a very weak acid (i.e. very little dissociation of HF into H^+ and F^-) which means that there are not very many hydrogen ions in the solution. With this in consideration, it would seem possible that better hydrogen termination of $(0001)_{Si}$ SiC surfaces could be achieved by HF solutions with lower pH (i.e. higher H^+ concentration). However, the experiments conducted using HCl:HF (pH=0.1) found this solution to also wet the SiC surface seemingly indicating that hydrogen termination of the $(0001)_{Si}$ SiC surface can not be achieved. The fact that solutions of higher OH^- concentration ($HF:NH_3OH$ (pH=8-9) and 7:1 NH_4F:HF (pH=4)) concentrations equally wetted the SiC surface points to the fact the $(0001)_{Si}$ 6H-SiC surface is terminated with OH rather than H. This agrees very well with the previously mentioned HREELS results of Starke *et al.* [41] which found OH^- groups at the $(0001)_{Si}$ surface. Unfortunately, these findings are completely opposite to what has been observed by MIRIRS (multiple internal reflection IR spectroscopy) and HREELS for Si (111) [42-45]. Using MIRIRS and HREELS, it has been found that for HF solutions of pH<7 a mixture of silicon hydrides (SiH, SiH_2, and SiH_3) are observed on the Si (111) surface. Further, MIRIRS studies have shown that for Si (111) hydrogen termination is achieved even using HF solutions with pH's as high at 10. By increasing the pH to $\geq$ 10, a Si (111) surface can be obtained which exhibits only silicon monohydrides (Si-H) [42-45]. Perhaps, MIRIRS is the technique of choice for studying the surface termination of SiC after HF dipping.

Finally, consideration must also be made of the presence of many steps on the vicinal $(0001)_{Si}$ 6H-SiC surface. It has been suggested that the observed oxygen levels after HF

dipping are due to more strongly bound oxides at the SiC steps. However, the results shown in Fig. 1 from Si (111) and $(0001)_{Si}$ 6H-SiC were taken from samples which were both off axis by 4-5° degrees in the same crystallographically equivalent directions. Ideally, these surfaces would have similar step densities and the argument could be made that the steps are not responsible for the observed oxygen levels. In reality, the number and nature of steps on the Si (111) and $(0001)_{Si}$ 6H-SiC surfaces are completely different. At a SiC step, both a carbon and a silicon atom are exposed allowing oxygen to be bonded to both these atoms instead of just to silicon as on Si (111). As HF is not known to remove oxides from diamond, oxygen at a silicon carbide step may be equally difficult to remove by HF. Also recent STM images of $(0001)_{Si}$ surfaces show a plethora of steps and risers with heights ranging from 3-12 monolayers high (i.e. 15-40Å) This exposes a significant amount of the (11-20) and (10-10) surfaces. In contrast, off axis Si (111) wafers exhibit only steps of two monolayers and do not significantly expose the (001) and (011) surfaces. Therefore it is possible for the (11-20) and (10-10) surfaces to be responsible for the observed oxygen. The AES spectrums of the (11-20) and (10-10) surfaces shown in Fig. 7(b,c) do show oxygen levels equal to those of the $(0001)_{Si}$ surface confirming this as a possibility. However, the authors feel that the step densities even on SiC are still to small to account for the all the oxygen observed on the $(0001)_{Si}$ surface after HF dipping. Further, if oxygen is harbored at the steps of SiC surfaces, less oxygen should be detected for on axis SiC wafers than for vicinal surfaces and this has not been observed.

UV/Ozone. Figures 5 and 6 show that UV/ozone oxidation treatment of SiC surfaces does not remove all of the non-carbidic carbon from (0001)Si 6H-SiC surfaces but does oxidize the SiC surface. This is shown via the appearance of a chemically shifted Si 2p peak and the downward shifting of the non-carbidic C 1s peak. This result is contradictory to what has been observed for UV/Ozone cleaning of Si and GaAs surfaces [21,22]. Although definite explanation for this observation is not yet at hand, the authors feel that using deeper UV lamps such as D_2 or Xe with or without the Hg lamp may work better for SiC. This is based on the assumption that generation of electron-hole pairs may assist the oxidation and removal non-carbidic carbon. As 6H-SiC has a much larger bandgap than both Si and GaAs (3.0 vs 1.1 and 1.4 eV), the higher energy light from the D_2 and Xe lamps may be more efficient at generating electron-hole pairs in SiC.

$(000\text{-}1)_C$ 6H-SiC. For $(0001)_C$ HF dipped surfaces, similarities to $(0001)_{Si}$ surfaces after HF dipping were observed. First, (1×1) LEED patterns from the $(000\text{-}1)_C$ surface were obtained after HF dipping which were similar to those found from the $(0001)_{Si}$ surface after HF dipping. Additionally, similarities in the oxygen and non-carbidic carbon levels were found. However, the nature of the oxygen and non-carbidic carbon were found to be significantly different. First, the position of the O 1s core level from the $(0001)_C$ surface was

found at 532.5 eV instead of 533.1 eV as for $(0001)_{Si}$. The value of 532.5 eV for the O 1s position on the $(0001)_C$ surface is very close to that observed from both CVD and natural diamond surfaces. Given the lower Si/C ratio, this strongly indicates that for the $(000\text{-}1)_C$ surface (and possibly the $(0001)_{Si}$ as well) all the surface oxygen is bonded to carbon instead of silicon.

The nature of the non-carbidic carbon for the $(000\text{-}1)_C$ surface after HF dipping was also observed to be different from that on the $(0001)_{Si}$ surface. Both EELS and XPS indicated that the non carbidic carbon on the $(000\text{-}1)_C$ face after HF dipping was much closer in nature to graphite. Looking at Table III, the C 1s value of 285.0 eV measured from noncarbidic carbon on the $(000\text{-}1)_C$ surface agrees exactly with previously published values measured from benzene and benzene related compounds. As benzene with its six fold ring shape is similar to graphite, it would not be unreasonable to expect to observe a π-π^* transition similar to that of graphite in EELS. This all suggests that the non-carbidic carbon observed on the $(000\text{-}1)_C$ face after HF dipping is related to benzene related and other similar hydrocarbons. Perhaps a detailed analysis of the π-π^* transition in organic molecules can be used to more accurately determine the nature of the non-carbidic carbon for both the $(000\text{-}1)_C$ and $(0001)_{Si}$ surfaces.

(11-20) and (10-10). The (11-20) and (10-10) surface exhibited results intermediary to those found for the $(0001)_{Si}$ and $(000\text{-}1)_C$ surfaces. AES spectrums of both surfaces revealed the Si/C ratios to be exactly equal to those found for the $(0001)_{Si}$ surface. Further, XPS of the (11-20) surface found the Si 2p and C 1s core levels positions for this surface to be the same as those found for the $(0001)_{Si}$ surface. In contrast, EELS spectrums taken from the (11-20) and (10-10) surfaces looked almost exactly like those taken from the $(000\text{-}1)_C$ surface both exhibiting loss peaks at 5 eV due to non carbidic carbon of benzene like origin. XPS of the non-carbidic C 1s peak from the (11-20) surface also exhibited was also similar to that observed from the $(000\text{-}1)_C$ surface. The fact that the non-polar (11-20) and (10-10) surfaces exhibit split similarities between the polar $(0001)_{Si}$ and $(000\text{-}1)_C$ surfaces is rather surprising.

From the above discussion it appears evident that unlike Si (111), a hydrogen terminated silicon surface for $(0001)_{Si}$ 6H-SiC is not achieved by dipping in 10% HF. Owing to the presence of Si-C backbonds, the outermost silicon surface atoms of the $(0001)_{Si}$ surface are extremely unstable in HF and are removed/etched away by the HF leaving a carbon rich surface terminated with a mixture of C-O and C-H bonding. This begs the question: Is there an *ex situ* cleaning procedure which can eliminate the C-O bonding and or remove the non-carbidic carbon? A review of diamond research unfortunately indicates that the only "wet chemical" found to achieve hydrogen termination of diamond is surprisingly, olive oil.

E. Conclusions

Wet chemical cleaning of 6H-SiC surfaces was investigated. HF based wet cleans were found to leave carbon rich SiC surfaces which were hydrophilic in nature. The hydrophilic

nature of these SiC surfaces suggests that HF dipping does not produce a hydrogen terminated SiC surface analogous to HF dipped Si surfaces. UV/Ozone oxidation was investigated as a means of removing non-carbidic carbon from 6H-SiC surfaces. UV/ozone exposure was not found to completely remove all non-carbidic carbon from the SiC surface. The UV/O_3 treatment, however, did induce a change in the chemical state of the non-carbidic carbon. This was seen in XPS via a shift in the non-carbidic carbon C 1s peak from 285.7 to 285.2 eV.

F. Future Research

Research to be conducted in the next reporting period includes:

- Investigation of UV/ozone cleaning of SiC with D_2 and Xe lamps,
- Investigation of use of Si capping layers on 6H-SiC as a passivating layer in *ex situ* cleaning, and
- Investigate difluoro-dioxygen (FOOF) as a wet chemical clean for SiC surfaces.

G. References

1. R. F. Davis, G. Kelner, M. Shur, J. Palmour, J. A. Edmond, Proc. of the IEEE, **79** 677 (1991).
2. See for example: S. Strite and H. Morkoc, J. Vac. Sci. and Technol. B **10**, 1237 (1992); J. H. Edgar, J. Mater. Res. **7**, 235 (1992); R. F. Davis, Proc. of IEEE **79**, 702 (1991), H. Morkoc and S.N. Mohammad, Science **267**, 51 (1995).
3. W. Kern, J. Electrochem. Soc. **137**, 1997 (1990).
4. R. Williams, *Modern GaAs Processing Methods*, 2nd ed. (Artech House, Inc., New York, 1990), pp. 81-114.
5. G. R. Srinivasan and B. S. Meyerson, J. Electrochem. Soc. **134** (6), 1518 (1987).
6. B. S. Meyerson, E. Ganin, D. A. Smith, and T.N. Nguyen, J. Electrochem. Soc. **133** (6), 1232 (1986).
7. C. Galewski, J. Lou, W. G. Oldham, IEEE Transactions on Semiconductor Manufacturing **3** (3), (1990).
8. M. Racanelli, D. W. Greve, M. K. Hatalis, L. J. van Yzendoorn, J. Electrochem. Soc. **138** (12), 3783 (1991).
9. J. H. McFee, R. G. Swartz, V. D. Archer, S. N. Finegan, and L. C. Feldman, J. Electrochem. Soc. **130** (10), 3083 (1989).
10. A. J. Pidduck, D. J. Robbins, A. G. Cullis, D. B. Gasson, and J. L. Glasper, J. Electrochem. Soc. **136** (10), 3083 (1989).
11. F. Ren, A. B. Emerson, S. J. Pearton, T. R. Fullowan, and J. M. Brown, Appl. Phys. Lett. **58** (10), 1030 (1991).
12. M. Kodama, Electronics Letters **30** (1), 89 (1994).
13. L. L. Yeh, Y. Xie, and P. H. Holloway, J. Appl. Phys. **65** (9), 3568 (1989).
14. Z. L-Weber, N. Newman, J. Washburn, and E. R. Weber, Appl. Phys. Lett. **54** (4), 356 (1989).
15. K. Prasad, Vacuum **46** (2), 127 (1995).
16. A. Zangwill, *Physics at Surfaces*, (Cambridge University Press, New York, 1988) pp. 221-231.
17. Y. T. Yeow, D. R. Lamb, and S. D. Brotherton, J. Phys. D: Appl. Phys. **8**, 1495 (1975).
18. E. H. Rhoderick, and R. H. Williams, *Metal-Semiconductor Contacts*, 2nd ed. (Oxford University Press, New York, 1988), pp. 5-17.

19. E. H. Snow, A. S. Grove, B. E. Deal, and C. T. Sah, J. Appl. Phys. **36** (5), 1664 (1965).
20. E. Yon, W. H. Ko, and A. B. Kuper, IEEE Trans. Electron Devices **13** (12), 276 (1966).
21. B.S Meryson, F. J. Himpsel, and K. J Uram, Appl. Phys. Lett. **57**, 1034 (1990).
22. M. Grundner and H. Jacob, Appl. Phys. A **39**, 73 (1986).
23. J. A. McClintock, R. A. Wilson, and N. E. Byer, J. Vac. Sci. Technol. **20**, 241 (1982).
24. R. F. Kopf, A. P. Kinsella, and C. W. Ebert, J. Vac. Sci. Technol. B **9**, 132 (1991).
25. Atomic Layer Epitaxy of Group IV Materials: Surface Processes, Thin Films, Devices and Their Characterization, Semiannual Technical Report, R. F. Davis, Grant #N00014-91-J-1416, Office of the Chief of Naval Research, July 1994.
26. F. Bozso, J. Muehlhoff, M. Trenary, W. J. Choyke, and J. T. Yates Jr., J. Vac. Sci. Technol. **A2** (3), 1272 (1984).
27. A. N. Andreev, M. M. Anikin, A. L. Syrkin, V. E. Chelnokov, Semiconductors **28** (6), 577 (1994).
28. S. Nakanishi, H. Tokutaka, K. Nishimori, S. Kishida, and N. Ishihara, Applied Surface Science **41/42**, 44 (1989).
29. L. M. Porter, J. S. Bow, M. J. Kim, R. W. Carpenter, and R. F. Davis, J. Mater. Res. **10** (3), 668 (1995).
30. R. E. Thomas, R. A. Rudder, and R. J. Markunas, J. Vac. Sci. and Technol. A **10**, 2451 (1992).
31. V. S. Smentkowski, J. Jansch, M. A. Henderson, J. T. Yates Jr., Surface Science **330**, 207 (1995).
32. O. M. Kuttel, L. Diederich, E. Schaller, O. Carnal, L. Schlapbach, Surface Science **337** L812, (1995).
33. Hollinger and Himpsel, Appl. Phys. Lett. **44**, 93 (1984).
34. A. Miyauchi, Y. Inoue, M. Ohue, N. Momma, T. Suzuki, and M. Akiyama, J. Electrochem. Soc. **137**, 3257 (1990).
35. A. Miyauchi, Y. Inoue, T. Suzuki, M. Akiyama. Appl. Phys. Lett. **57**, 676 (1990).
36. Personnel Communication with Jacob van der Weide.
37. S. V. Didziulis, J. R. Lince, P. D. Fleischauer, and J. A. Yarmoff, Inorg. Chem. **30**, 672 (1991).
38. S. Verhaverbeke, I. Teerlinck, C. Vincker, G. Stevens, R. Cartuyvels, and M.M. Heyns, J. Electrochem. Soc. **141** 11, 2852 (1994).
39. J. S. Judge, J. Electrochem. Soc. **118** 11, 1773 (1971).
40. M. Dayan, Surface Science **149**, L133 (1985).
41. U. Starke, Ch. Bram, P.-R. Steiner, W. Hartner, L. Hammer, K. Heinz, and K. Muller, Appl. Surf. Sci. **89**, 175 (1995).
42. T. Suzuki ans S. Adachi, Jpn. J. Appl. Phys. **33**, 5599 (1994).
43. L. Li, H. Bender, T. Trenkler, P. W. Mertens, M. Merius, W. Vandervorst, and M.M Heyns, J. Appl. Phys. **77**, 1323 (1995).
44. G. S. Higashi, R. S. Becker, Y. J. Chabal, A. J. Becker, Appl. Phys. Lett. **58**, 1656 (1991).
45. G. S. Higashi, Y. J. Chabal, G. W. Trucks, and K. Raghavachari, Appl. Phys. Lett. **56**, 656 (1990).

IV. Development of a System for Integrated *In Situ* Surface Cleaning and Oxide Formation on 6H-SiC

A. Introduction

The development of high-temperature, -power and -frequency devices based on SiC requires a more complete understanding of the oxide formation and interface characteristics. By using an integrated UHV system that contains: remote plasma cleaning, HF vapor phase oxide removal, and various oxide deposition capabilities, interfaces with lower contaminant levels will be prepared as a better understanding of the SiC oxide formation process is gained. The UHV-compatible cleaning and oxide formation system will be integrated with an advanced system that includes other processing and characterization capabilities. The UHV surface characterization system will allow for *in vacuo* characterization of the SiO_2/SiC interface and oxides grown by various individual and combination processes.

B. Experimental Procedure

The integrated system will allow for most of the characterization to be accomplished without exposing samples to the ambient. Furthermore, the processes will be characterized at various stages, thus allowing for the understanding of the entire oxidation process. A typical process is given as follows: (1) the native oxide is removed via the HF vapor system; (2) the sample is cleaned using a hydrogen plasma; (3) the sample is characterized using the various systems available: Raman spectroscopy, UV photoemission, LEED/Auger, UPS, and XPS; and (4) the oxide layer is deposited using a combination of thermal or plasma CVD. The H-plasma step removes any residual contaminants left after the HF cleaning and results in a H-terminated surface. Then *in vacuo* characterize the various grown oxide layers in order to determine the characteristics of the different growing techniques.

The unique capability that will be employed in this study is an integrated processing system with *in situ* diagnostics. The system is shown schematically in Fig. 1. The system includes advanced surface characterization, surface preparation, and growth capabilities. Also included is the development of a UHV CVD/oxidation system which would be constructed to be compatible with the integrated system. The system is based on a UHV linear sample transfer mechanism. This transfer chamber which is 35 ft. long, connects eight separate surface preparation, processing or characterization chambers. Techniques relevant to this study include the remote plasma surface preparation chamber, LEED, AES, XPS, uv-photoemission, thermal desorption, and AlN deposition. Other chambers which could prove useful include *in situ* Raman spectroscopy and Si MBE.

The oxide deposition and hydrogen plasma apparatus have progressed past the design phase and are currently in construction. The system will have a cryopump to maintain a base

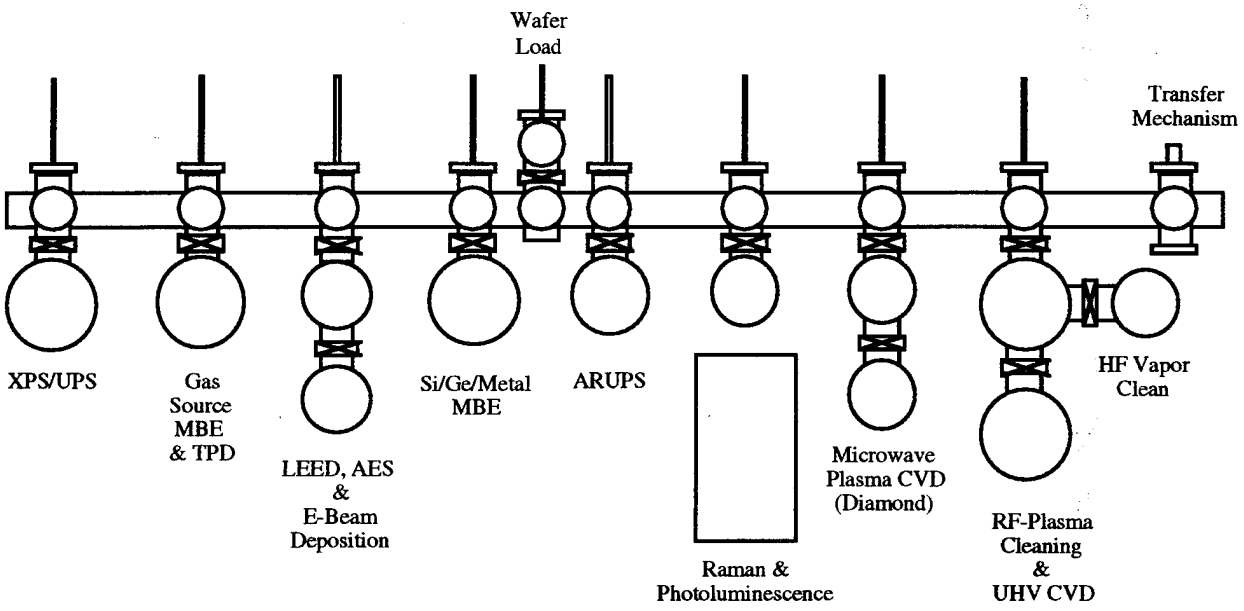

Figure 1. Schematic of the integrated growth and characterization system to be employed in the studies of defects in insulators on SiC.

pressure of $10^{-8} - 10^{-9}$ torr to ensure low contamination. By maintaining such a low base pressure, a nearly contaminant-free growth chamber for every growth cycle can be achieved. To further ensure the quality of deposition, the system will have a residual gas analyzer to examine the quality of gases used in the deposition process and give an accurate account of the composition of the deposited oxide. A Langmuir probe is used to measure the characteristics of the plasma for plasma enhanced CVD (PECVD). A schematic of the system is shown in Fig. 2. The deposition chamber will have a substrate temperature range to 1250°C. The plasma for PECVD will have a power range to 400 Watts enabling the process to be varied from rapid thermal oxidation to CVD deposition to PECVD in the same chamber. It is possible to perform *in situ* and *in vacuo* diagnostics at various points in the oxide growth process. Using this method, investigation will occur on how the deposition processes effect the SiO_2 surface and interface of the SiC/SiO_2. Also to be investigated are the characteristics of the different oxides grown by the different methods. It is hoped to gain insight into the surface chemistry of the different growth processes and the quality of oxide grown. By maintaining this versatility in the system design, the chamber can be adapted and new avenues explored as they become apparent.

C. Conclusions

The integrated UHV system will be able to explore processes that have previously been unobtainable. The uniqueness of the cleaning system integrated with the growth and

characterization system allows for capabilities that have not been previously used in the characterization and growth of oxides on SiC.

D. Future Research Plans and Goals

There will be considerable focus on the examination of the oxide layers for use as gate insulators in field effect devices. A process by which the gate oxide and gate can be applied to an industrial setting will be attempted.

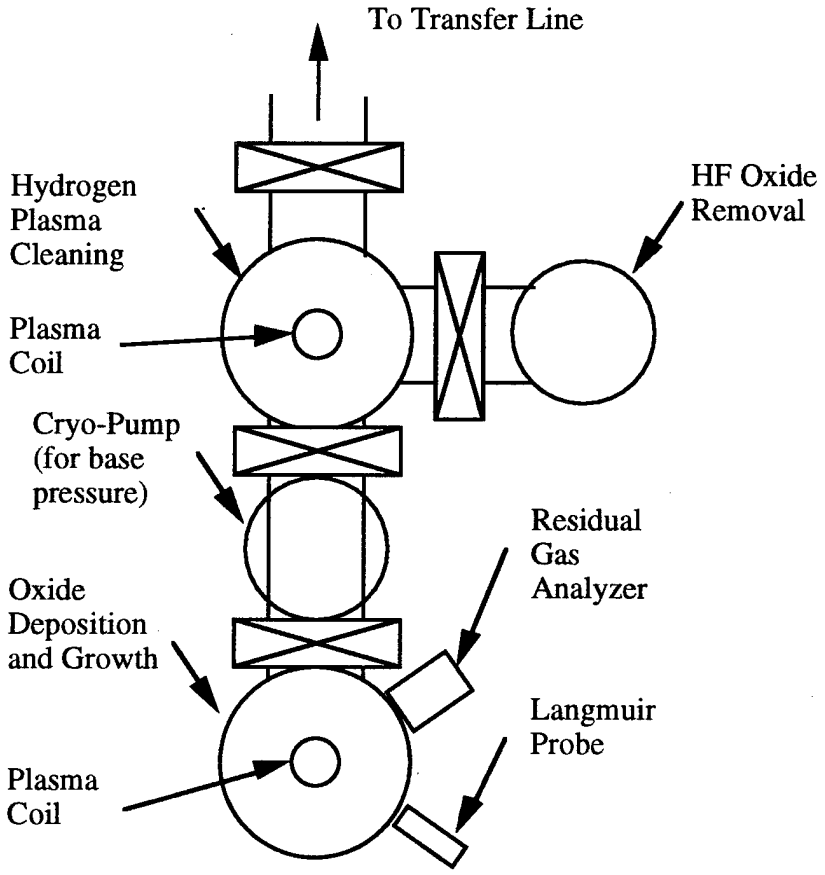

Figure 2. Schematic of oxide deposition and hydrogen plasma system with residual gas analyzer and Langmuir probe.

V. Characterization of Oxides on N- and P-Type 4H- and 6H-SiC

A. Introduction

Silicon carbide (SiC) has been shown to be an excellent material for the fabrication of devices for high-power, high-frequency and high-temperature applications [1]. The advantages of SiC metal oxide semiconductor field effect transistors (MOSFETs) has also been discussed [2]. The successful operation of these devices hinges on the interface and bulk properties of the gate dielectric, usually an oxide. Previous researchers have reported results on thermally grown oxides on N-type [3-6] and P-type 6H-SiC [5, 7-11]. While the results obtained on N-type 6H-SiC have shown that those oxides are of high quality, oxides grown on P-type 6H-SiC exhibit large flatband voltage shifts and are thus unsatisfactory for application as gate dielectrics. Oxides deposited under special conditions with surface preparation specific to the particular deposition might show improved interfacial properties over thermally grown oxides.

The SiO_2-SiC interfaces will be characterized using capacitance-voltage (C-V) measurements [12]. A Mask set was designed to fabricate the MOS structures required for accurate and complete electrical characterization. It is proposed to study the properties of thermally grown oxides on 6H-SiC and 4H-SiC until wafers are obtained with oxides deposited by Prof. Nemanich's group with the specific pre-deposition surface treatments and deposition conditions.

B. Experimental Procedure

The proposed process to fabricate the MOS capacitors and the gated diodes is described in this section. The wafer will be subjected to a sacrificial oxidation to clean the surface. A low temperature oxide (LTO) of thickness 6000A will be deposited on the wafer. This oxide will then be patterned so that the regions to receive the N^+ implant are exposed. Another layer of LTO of thickness 1000A will be deposited on the wafer. This 1000A of oxide acts as a pad oxide during the implant step. The patterned wafer will be subjected to a nitrogen implant to form the N^+ highly doped regions. The wafer will be then subjected to a high temperature anneal to activate the dopant. The oxide will be further patterned to define the gate region and the gate dielectric thermally grown or deposited on the SiC. A blanket deposition of polysilicon will be then done and heavily doped N^+ *in situ* with $POCl_3$. The poly will be then patterned to form the gate. Using the poly as a mask, the gate dielectric not covered by the poly will be etched off. Ti/Al will be then deposited and patterned by lift-off to form the metal contacts to the poly and the N^+ source. A large area backside blanket evaporation of Al will be done to form an ohmic contact.

A set of experiments is being performed to obtain LTO deposition conditions on the 1.125" diameter SiC wafers. The deposition conditions of the furnace for LTO deposition have been

evaluated only for 4" silicon wafers placed vertically in quartz boats inside the furnace tube. The SiC wafers will be placed on top of the 4" silicon wafer which would be placed horizontally on the quartz boat in the furnace. Due to this altered configuration of wafers inside the furnace, the gas flows and temperature gradients will be altered, changing the deposition. Therefore, deposition conditions need to be evaluated for the smaller diameter SiC wafers. It is hoped to obtain an LTO uniformity of about 5-10% over the area of the SiC wafer. Silicon wafers of 1" are being used instead of SiC wafers to obtain and define the deposition conditions.

C. Discussion

The design of the four-level Mask set was completed in the last quarter. The first level of the Mask set will be used to define the area receiving the N^+ nitrogen implant required for the source regions of the MOS-gated diodes. The second level of the Mask set will be used to define the area of the SiC on which the gate oxide would be thermally grown or deposited. In other words, this level would act as the active area mask. The third level of the Mask set will be used to define the polysilicon gate regions and the fourth level of the Mask set will be used to define the metal regions for contacts and pads. The order for the Mask set was placed with DuPont Photomasks Inc. Included in this order was a request for paper plots of the four levels. The plots of the four levels were received and checked to conform exactly to the design. The delivery of the actual Mask set (glass plates) is expected shortly from DuPont.

An order for 6H-SiC and 4H-SiC wafers from CREE Research Inc. was placed. The fabrication of the MOS devices will be on these wafers. Receipt of these wafers is expected in 4-6 weeks. Device fabrication will begin on receipt of the wafers.

D. Conclusions

A Mask set was designed to fabricate devices that would enable accurate characterization of the SiO_2-SiC interface. Devices to be fabricated include MOS capacitors and MOS gated diodes. The wide bandgap of SiC and the attendant modifications that this fact introduces in the characterization of the interface as opposed to the characterization of the SiO_2-Si interface have been recognized. The order for the Mask set was placed with DuPont Photomasks Inc. The paper plots of the four Mask levels were received and checked to conform exactly with the Mask layout.

E. Future Research Plans and Goals

Once the Mask set and the SiC wafers have been received, devices will be fabricated on thermal oxide using an previously developed process and the SiO_2-SiC interface will be characterized.

F. References

1. R. J. Trew, J-B. Yan and P. M. Mock, Proc. IEEE **79**, 598 (1991).
2. M. Bhatnagar and B. J. Baliga, IEEE Trans. on Electron Devices **40**, 645 (1993).
3. A. Suzuki, H. Ashida, N. Furui, K. Mameno and H. Matsunami, Jpn. J. Appl. Phys. **21**, 579 (1982).
4. D. Alok, P. K. McLarty and B. J. Baliga, Applied Phys. Lett. **64**, 2845 (1994).
5. T. Ouisse, N. Becourt, C. Jaussaud and F. Templier, J. Appl. Phys. **75**, 604, (1994).
6. P. Neudeck, S. Kang, J. Petit, and M. Tabib-Azar, J. Appl. Phys. **75**, 7949 (1994).
7. C. Raynaud, J-L. Autran, B. Balland, G. Guillot, C. Jaussaud and T. Billon, J. Appl. Phys. **76**, 993 (1994).
8. D. Alok, P. K. McLarty and B. J. Baliga, Appl. Phys. Lett. **65**, 2177 (1994).
9. J. N. Shenoy, G. L. Chindalore, M. R. Melloch, J. A. Cooper Jr., J. W. Palmour and K. G. Irvine, J. Electronic Mat. **24**, 303 (1995).
10. J. N. Shenoy, L. A. Lipkin, G. L. Chindalore, J. Pan, J. A. Cooper Jr., J. W. Palmour and M. R. Melloch, *Proc. 21st Intl. Symp. on Compound Semiconductors*, 499 San Diego (1994).
11. S. T. Sheppard, M. R. Melloch and J. A. Cooper Jr., IEEE Trans. on Electron Devices **41**, 1257 (1994).
12. E. H. Nicollian and J. R. Brews, *MOS Physics and Technology*, Wiley (1991).
13. A. Goetzberger and J. C. Irvin, IEEE Trans. on Electron Devices **15**, 1009 (1968).

VI. Measurement of Minority Carrier Diffusion Length in Silicon Carbide

A. Introduction

Silicon carbide has been projected to be an excellent semiconductor for high-power, high-frequency and high-temperature applications [1,2]. Minority carrier diffusion length in a semiconductor is a very important parameter for design, understanding or modeling of devices [3]. One of the methods for the determination of the bulk minority carrier diffusion length in a semiconductor is shown in Fig. 1 [4]. It utilizes an electron beam incident on the semiconductor surface adjacent to a current collecting Schottky barrier. The planar configuration can also be used for imaging defects. It enables a direct correlation to be made between the characteristics of defects and material parameters.

The principle of operation is as follows: electron-hole pairs are generated by the impact of the primary electrons of energy E_0 on the semiconductor. These carriers either recombine after diffusing through a certain distance or reach the edge of the depletion region around the Schottky barrier diode where they are immediately swept away by the built-in field and collected as EBIC current. As the beam is slowly moved away from the diode, the EBIC current (I), decays with the beam to depletion edge distance, x, according to the relationship.

$$I=I_0\exp(-x/L) \tag{1}$$

The diffusion length can thus be extracted from slope of a plot of $\ln(I/I_0)$ vs x.

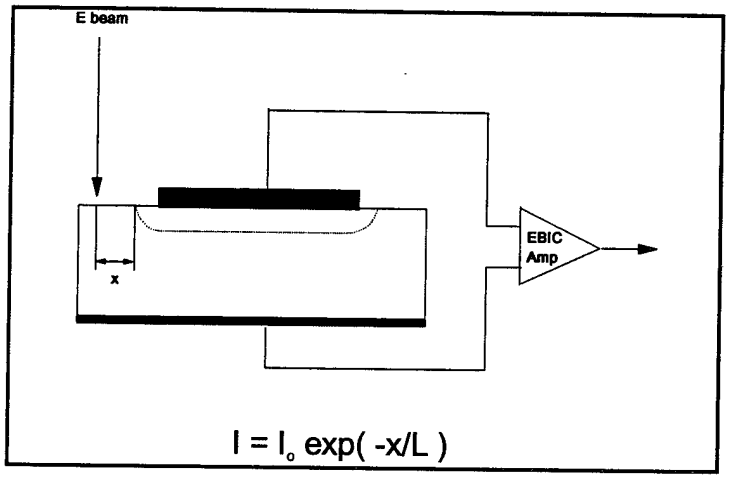

Figure 1. Planar configuration used for the measurement of minority carrier diffusion length.

B. Experimental Setup

The setup used for the measurement of diffusion length is shown in Fig. 2. The electron beam is scanned along the desired region on the surface, such that the point of approach is at least two diffusion lengths away from the depletion edge. The direction of approach must be perpendicular to the edge of the depletion region. The scanning circuit in the microscope controlling the rastering of the electron beam is used to trigger the oscilloscope as shown. Carriers are generated by the incident electron beam and these carriers diffuse to the depletion region. This current is collected, amplified and outputted by the EBIC amplifier to the oscilloscope. A plot of EBIC current vs the time is obtained on the oscilloscope. The oscilloscope is interfaced to the PC through a GPIB card and, hence, the data from the oscilloscope can be downloaded on to the PC for interpretation.

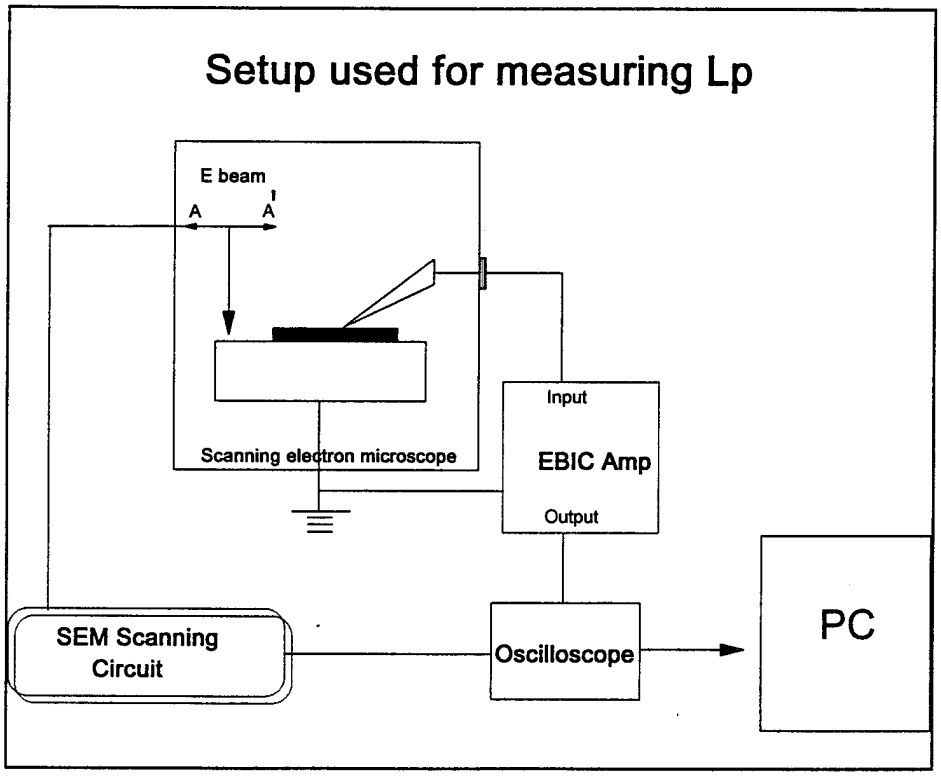

Figure 2. Setup used for measuring minority carrier diffusion length in SiC.

The secondary electron image is very useful for determining the position of the metal edge. It is very critical to scan the beam very close to the depletion edge while dealing with very small diffusion lengths. The scan rate is also determined using the secondory electron image. The diameter of the Schottky diode is ascertained using the SEM in the secondary electron mode. The time taken for the beam to scan the diode is obtained from the plot on the oscilloscope and

hence the scan rate is calculated. Using the scan rate, the time on the x axis is converted to a distance, x. A plot of the distance x vs the natural log of the normalized EBIC current (I/I_{max}) is thus obtained. The inverse of the slope of the linear region of the plot gives the diffusion length.

C. Results

Diffusion lengths were calculated for both 6H and 4H-SiC. Ti/n-SiC Schottky barrier diodes were fabricated on both 4H and 6H-SiC [5,6] and these diodes were used for the analysis. Figure 3 shows a typical plot obtained from the oscilloscope for any scan. It is observed that far from the depletion edge, the EBIC current is almost constant and can be approximated to a zero current. As the depletion edge is approached, notice that the current increases exponentially. This is the region of interest. A typical plot of ln (I/I_0) vs x is shown in Fig. 4. The inverse of the slope of such a plot gives the minority carrier diffusion length of the semiconductor. Using the approach mentioned above, diffusion lengths were calculated at various locations across a wafer on 4H and 6H-SiC. Table I shows the results of the measurements made on 6H-SiC. The average value of the minority carrier diffusion length obtained for the sample was 0.40 μm. There was a 35% variation in the diffusion length over one quadrant of the wafer. Table II shows the measurements made on 4H-SiC. In 4H-SiC, the average value of the diffusion length for holes was measured to be 1.46 μm. The variation in diffusion length was estimated to be 15% over one quadrant of the wafer. W. J. Schaffer reported that hole mobilities in 4H-SiC was 20-30% higher than in 6H-SiC [7]. Based on the values reported for hole mobilities, lifetimes were calculated to be 0.62 nsec in 6H-SiC and 5.5 nsec in 4H-SiC. All wafers were obtained from CREE Research, Inc.

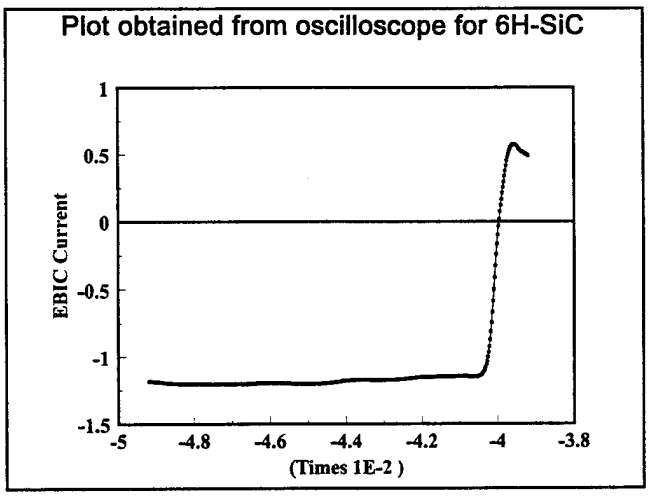

Figure 3. A typical plot obtained from the oscilloscope for an EBIC line scan on a 6H-SiC diode.

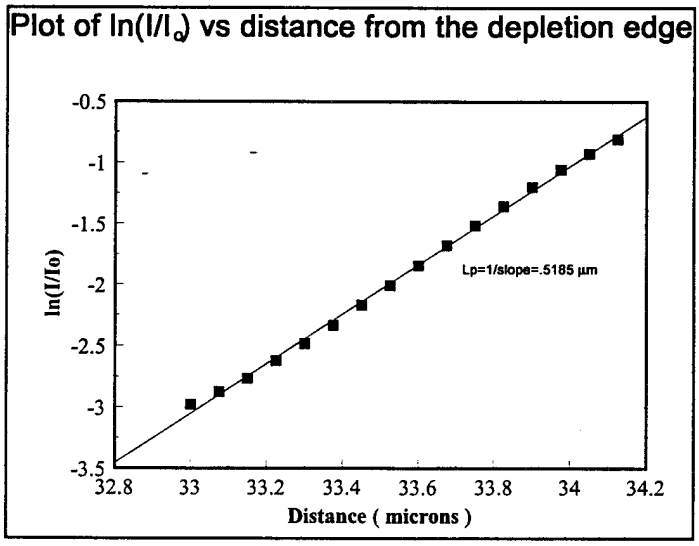

Figure 4. Plot of ln (I/I_0) vs distance, x, from the depletion edge for a 6H-SiC Schottky diode

Table I. Values of Hole Diffusion Length Obtained for 6H-SiC over Different Locations on the Wafer

No.	Accelerating Voltage	Diffusion Length
1.	5 keV	.259056
2.	5 keV	.469439
3.	5 keV	.461541
4.	5 keV	.291022
5.	5 keV	.494299
6.	5 keV	.406092
7.	5 keV	.424218
8.	6 keV	.285023
7.	6 keV	.327222
8.	6 keV	.367751
9.	6 keV	.384129
10.	7 keV	.50158
11.	7 keV	.465246
12.	7 keV	.45824

Mean Lp = .3989 microns Max Variation = 35%

D. Discussion

The analysis given above is based on a number of assumptions and approximations. Some of which may impose restrictions on the use of the technique and should therefore be discussed. First the sample is considered semi infinite, i.e., bounded only by the top surface. In practice if the sample is large enough so that when the linescans are performed, the beam can

Table II. Values of Hole Diffusion Length Obtained for 4H-SiC over Different Locations on the Wafer

No.	Accelerating Voltage	Diffusion Length
1.	4 keV	1.573493
2.	4 keV	1.59746
3.	4 keV	1.469098
4.	5 keV	1.436566
5.	5 keV	1.391311
6.	5 keV	1.57635
7.	5 keV	1.50848
8.	6 keV	1.647429
7.	6 keV	1.352555
8.	6 keV	1.517838
9.	6 keV	1.520497
10.	7 keV	1.241067
11.	7 keV	1.323984
12.	7 keV	1.232296

Mean Lp = 1.45631 microns Max Variation = 13%

always be kept well away from the sample ends, and if the thickness of the sample is large compared to the diffusion length, the assumption can be assumed valid. Since these conditions are met, we can assume the hypothesis to be correct.

Secondly the collecting diode is also assumed to be semi-infinite. This condition can be easily satisfied if the diameter of the diode is more than 10 times the diffusion length which is the case here and, hence, this assumption is assumed valid.

Thirdly, the relation (1) is valid only if the generated carriers are separated by the built-in field of a vertical junction, therefore, the effect of the horizontal part of the junction is negligible. The minority carrier diffusion length in the lateral direction is obtained from this measurement. Since there is anisotropy in SiC, it is important to ensure that the generation volume is close enough to the surface so as to make the contribution from the vertical direction negligible. The generation volume can be approximated as a sphere of diameter R_G called the Grun radius, which is given by the relation:

$$R_G=(0.0398*E_0^{1.75})/\rho \qquad (2)$$

where ρ is the density of the material, and E_0 is the energy of the beam in kV. The location of the maximum generation of carriers is at a distance z from the surface ($\sim 0.41 \times R_G$). Keeping in mind these factors, beam energy of 5 kV was chosen which would give us a R_G of 0.2 μm.

Finally, an important consideration in the measurement was surface recombination velocity. Some of the generated carriers can recombine at the semiconductor surface before reaching the

depletion edge. The effect of surface recombination velocity (v_s) influences the diffusion equation in the following manner.

$$I=I_0(x^{\alpha})\exp(-x/L) \tag{3}$$

where α=-1/2 for v_s=0 and α=-3/2 for v_s=inf. This equation is generally accurate for x >2L and since our measurement is usually confined to regions x < 2L we can neglect the correction factor. However to confirm this, a curve fit was done for various values of α and it was found to have very little effect on the extracted value of L_p as shown in Fig. 5.

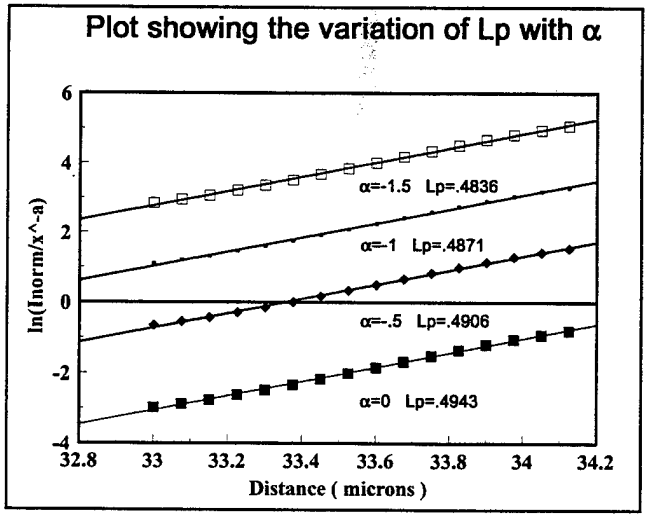

Figure 5. Plot showing the variation of the minority carrier diffusion length in 6H-SiC with α

E. Conclusions

A useful SEM-EBIC technique for measuring the minority carrier diffusion length has been set up. Minority carrier diffusion lengths have been measured in both 4H and 6H-SiC. The minority carrier diffusion length in 6H-SiC was found to be 0.40 μm and, that is, 4H-SiC was found to be 1.46 μm. Lifetimes calculated from based on the values for hole mobilities reported in 4H and 6H-SiC were estimated to be 0.62 nsec in 6H-SiC and 5.5 nsec in 4H-SiC.

F. Future Research Plans and Goals

Attempt will be made to measure the diffusion length of silicon carbide in the vertical direction in order to study anisotropy. This can be done by varying the energy of the beam and measuring the EBIC current from the sample. A curve fit between the collection efficiency of the junction and the energy of the beam gives an estimate of the minority carrier diffusion length.

G. References

1. B. J. Baliga, *Power Semiconductor Devices and Circuits*, Ed. by A. A. Jaecklin, Plenum Press, pp. 377, 1992
2. M. Bhatnagar and B. J. Baliga, IEEE Transactions on Electron Devices **40** (3), (1993).
3. A. Boudjani, G. Bassou, T. Benbakhti, M. Beghdad and B. Belmekki, Solid State Electronics **38** (2), 471 (1995).
3. V. K. S. Ong, J. C. H. Phang and D. S. H. Chan, Solid State Electronics **37** (1), 1 (1994).
4. D. E. Ionnou, and C. A. Dimitriadis, IEEE Transactions on Electron Devices, **29** (3), (1982).
5. D. Alok, B. J. Baliga, and P. K. McLarty, IEEE Electron Device Letters **15** (10), (1994).
6. R. Raghunathan, D. Alok, and B. J. Baliga, IEEE Electron Device Letters **16**, (6) (1995).
7. W. J. Schaffer, G. H. Negley, K. G. Irvine, and J. W. Palmour, Mat. Res. Soc. Symp. Proc. **339**, 1994.

VII. Rectifying and Ohmic Contacts for P-type Alpha (6H) Silicon Carbide

A. Introduction

While the wide bandgap of SiC is responsible for its use in opto-electronic, high-power, and high-temperature devices, this property also adds to the difficulty of controlling the electrical properties at the metal-semiconductor contacts in these devices. The primary parameter used to quantify the electrical relationship at these interfaces is the Schottky barrier height (SBH), or the energy barrier for electrons traversing the interface. A small SBH is desired for a contact which obeys Ohm's Law, while a relatively large SBH is necessary to create a good rectifying contact.

The formation of low resistivity and thermally stable ohmic contacts to 6H-SiC remains a serious problem in the development of SiC device technology. For SiC power devices to have the advantage over Si, the contact resistivities must be below 1×10^{-5} Ω-cm^2 [1]. In addition, the electrical characterization of state-of-the-art SiC films depends on the ability to fabricate ohmic contacts on material with low carrier concentrations. Therefore, better ohmic contacts are needed both for improving device performance and for improving the quality of films which can be grown. The thermal stability of ohmic contacts is of particular concern for p-type SiC, which have traditionally relied on Al or Al alloys to dope the SiC surface below the contacts. While the fabrication of ohmic contacts to SiC also has usually depended on very heavily-doped surfaces, the introduction of high levels of dopants in the near surface device region of the epilayer prior to the deposition of the contact or by ion implantation through the contact makes probable the introduction of point and line defects as a result of the induced strain in the lattice. Based on all of these issues and experiments already performed at NCSU, our goals are to produce contacts which are thermally stable and have low contact resistivities while also reducing the need for doping by ion implantation.

Low resistance contacts to p-type SiC remain a substantial challenge for high temperature and high-power devices. An Al-Ti alloy [2] annealed at 1000°C for 5 min. was reported to yield contact resistances ranging from 2.9×10^{-2} Ω cm^2 for a carrier concentration of 5×10^{15} cm^{-3} to 1.5×10^{-5} Ω cm^2 for 2×10^{19} cm^{-3}. The thermal stability of these contacts was not reported. Aluminum deposited on a heavily-doped 3C-SiC interlayer on a 6H-SiC substrate and subsequently annealed at 950°C for 2 min. reportedly yielded contact resistivities of $2\text{–}3\times10^{-5}$ Ω cm^2 [3]. Because of its low melting point (660°C), however, pure Al would be unsuitable for high temperature applications. Platinum contacts annealed from 450 to 750°C in 100°C increments were also used as ohmic contacts to p-type SiC [4]. These contacts, which rely on the combination of a highly-doped surface and the high work function of Pt, have not been known to yield contact resistivities as low as those for the contacts containing Al.

B. Experimental Procedure

Vicinal, single-crystal 6H-SiC (0001) wafers provided by Cree Research, Inc. were used as substrates in the present research. The wafers were doped with N or Al during growth to create n- or p-type material, respectively, with carrier concentrations of $1–5\times10^{18}$ cm^{-3}. Homoepitaxial layers (1–5 μm thick) grown by chemical vapor deposition (CVD) were Al-doped with carrier concentrations ranging from 1×10^{16} to 1×10^{19} cm^{-3}. The surfaces were oxidized to a thickness of 500–1000 Å in dry oxygen. The substrates were simultaneously cleaned and the oxide layer etched from the surface using a 10 min. dip in 10% hydrofluoric acid, transferred into the vacuum system, and thermally desorbed at 700 °C for 15 min. to remove any residual hydrocarbon contamination.

A UHV electron beam evaporation system was used to deposit the NiAl and Ni films. After depositing 1000 Å of NiAl, 500–1000 Å of Ni was deposited as a passivating layer. Pure Ni (99.99%) and pure Al (99.999%) pellets were arc melted to form alloyed pellets of 50:50 atomic concentration for evaporation of NiAl. The films were deposited onto unheated substrates at a rate of 10–20 Å/s. The pressure during the depositions was between 5×10^{-9} and 5×10^{-8} Torr.

Circular contacts of 500 μm diameter were fabricated for electrical characterization by depositing the metal films through a Mo mask in contact with the substrate. Silver paste served as the large area back contact. For contact resistance measurements, TLM patterns [6] were fabricated by photolithography. The Ni/NiAl films were etched in phosphoric acid : acetic acid : nitric acid (12 : 2 : 3) at 50 °C (etch rate ≈ 30 Å/s). The contact pads were 300×60 μm with spacings of 5, 10, 20, 30 and 50 μm. Mesas in the substrate were not fabricated. All subsequent annealing was conducted in a N_2 ambient in a rapid annealing furnace.

Electrical characteristics were obtained from current-voltage and capacitance-voltage measurements. Current-voltage (I-V) measurements were obtained with a Rucker & Kolls Model 260 probe station in tandem with an HP 4145A Semiconductor Parameter Analyzer. Capacitance-voltage (C-V) measurements were taken with a Keithley 590 CV Analyzer using a measurement frequency of 1 MHz.

Auger electron spectroscopy (AES) was performed with a JEOL JAMP-30 scanning Auger microprobe. The films were sputtered with Ar ions at a beam current and voltage of 0.3 μA and 3 kV, respectively, to obtain composition profiles through the thickness of the films.

C. Results

Modifications to Deposition System. To better control the deposition of compounds for SiC contacts by electron beam deposition, a second Leybold Inficon film thickness monitor was installed in the UHV chamber. Linear motion shifts on both thickness monitors allowed the monitors to be moved relative to the location of the deposition sources. Cylindrical material

directors placed around the crystals were used to try to isolate the flux reaching the crystal from one deposition source while eliminating the flux from the other source. As of this writing preliminary results have shown that some cross-deposition of material is inevitable, but it can probably be kept low enough to give satisfactory estimates of the amount of each material deposited while running both sources simultaneously. The necessity of having two thickness monitors will be elaborated in the Future Plans and Goals section of this report.

Chemical Characterization of As-deposited Films. An Auger depth profile of a film deposited from the NiAl source showed that the overall composition remained relatively stable. The relative compositions of Ni and Al were calculated by referencing to pure Ni and pure Al standards and accounting for their corresponding sensitivity factors. The average atomic composition was approximately 50:50.

Schottky Contacts. In the as-deposited condition the Ni/NiAl contacts were rectifying on p-type SiC with carrier concentrations of 1.6×10^{16} and 3.8×10^{18} cm^{-3} in the epilayer. The sample with the lower carrier concentration displayed leakage current densities of $\sim1\times10^{-8}$ A/cm^2 at 10 V and ideality factors between 1.4 and 2.4, while the latter sample displayed approximately five orders of magnitude higher leakage current densities and similar ideality factors. The average Schottky barrier heights (SBH's) calculated for the samples with the lower and higher carrier concentrations were 1.37 and 1.26 eV, respectively. The lower SBH calculated for the former sample is likely due to enhanced thermionic field emission through the upper energy region of the barrier because of the narrower depletion region. Hence, the 1.37 eV value is believed to be more accurate.

Similar results were obtained for as-deposited Ni and Au contacts on p-type ($2.1–4.5\times10^{16}$ cm^{-3}) 6H-SiC (0001). These samples displayed similar leakage currents and ideality factors of 1.3–2.1 and <1.1, respectively. From these measurements SBH's of 1.31 eV for the Ni contacts and 1.27 eV for the Au contacts were calculated. In comparison, as-deposited Ni on n-type (4.1×10^{16} cm^{-3}) 6H-SiC (0001) yielded ideality factors below 1.1, similar leakage current densities to those stated above, and SBH's of 1.14 eV and 1.21 eV calculated from I-V and C-V measurements, respectively.

Our measurements on p-type SiC have shown consistent differences from measurements on n-type 6H-SiC. The SBH's tended to be higher on p-type than on n-type material. While leakage currents for Au, NiAl, and Ni contacts on p-type 6H-SiC were comparable to Ni contacts on n-type 6H-SiC, the ideality factors were higher on p-type SiC. These ideality factors and SBH's are higher than for Ni contacts (and other previously studied contacts) on n-type 6H-SiC (0001). The higher ideality factors indicates that thermionic emission was not the dominant current transport mechanism in the p-type SiC and may indicate the occurrence of recombination at deep levels.

On the other hand, the relationship between the SBH's of the metals on p-type SiC and their respective work functions was similar to that which we previously found for n-type SiC. The calculated SBH's on p-type SiC are plotted vs. the metal work functions in Fig. 1. The work function for NiAl was taken to be the average of the work functions for pure Ni and pure Al since a value was not found in the literature for NiAl. The slope of the line fit to the empirical data was -0.16 as compared to a slope of -1.0 for the theoretical data. These results indicate that surface states on p-type 6H-SiC (0001) cause a partial pinning of the Fermi level, in agreement with the results of our previous, extensive study on n-type SiC.

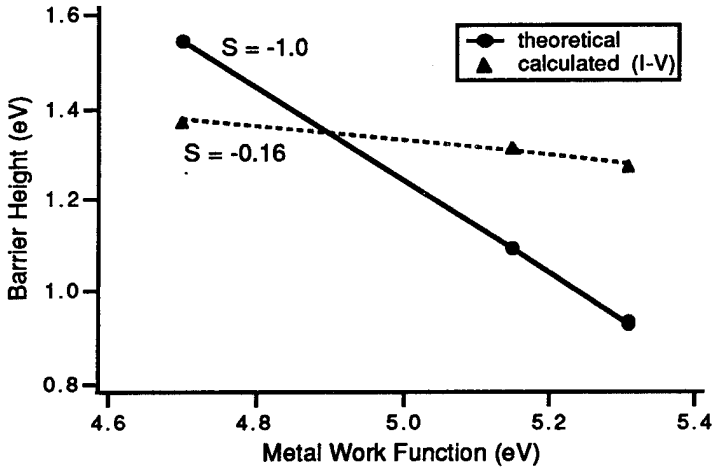

Figure 1. Graph of calculated and theoretical barrier heights of as-deposited NiAl, Ni, and Au contacts on p-type 6H-SiC vs. metal work function. The calculated values were determined from I-V measurements, and the theoretical values were calculated according to the Schottky-Mott limit. The slopes, S, of the lines fit to each set of data are indicated on the graph.

Ohmic Contacts. The Ni/NiAl contacts were sequentially annealed for total times of 10–80 s at 1000 °C in a N_2 ambient. This temperature was used because (1) limited intermixing of Al and SiC was reported at 900 °C [7] and (2) other papers report annealing in this temperature range for Al-based ohmic contacts on p-type SiC [2, 3, 8]. Because of the extremely high thermodynamic driving force for Al to form an insulating oxide layer (ΔG_f (Al_2O_3) ~ -1300 kJ/mol at 1000 °C [JANAF - Chase, M., *et al.*, JANAF Thermochem. Tables, 3d Ed. J. Phys. Chem. Ref. Data, 1985. 14(Supp. 1)]), 1000 Å of Ni was deposited on top of the NiAl contacts to slow the oxidation process.

Table I summarizes the results of I-V measurements taken at selected intervals through the annealing series for three samples with various carrier concentrations in the SiC epitaxial layer (1.4×10^{18}, 5.7×10^{18}, and 1.5×10^{19} cm^{-3}). The two samples with the lower carrier concentrations were not truly ohmic but became ohmic-like after annealing for 80 s. This annealing series will be continued to determine whether ohmic behavior in these two samples

will ensue; however, the additional force on the probes needed to obtain consistent results indicates that an oxide has begun to form at the surface and may cause problems with further annealing. The sample with the higher carrier concentration was ohmic after annealing for 10 s. The calculated specific contact resistivity remained approximately 2.0×10^{-2} Ω cm^2 through annealing for 60 s. A slight increase to 3.1×10^{-2} Ω cm^2 was calculated after annealing for 80 s. This increase is believed to be due to the surface oxide layer.

Table I. Estimated specific contact resistivities / electrical behavior of Ni (1000 Å) / NiAl (1000 Å) / p-SiC after annealing at 1000 °C for 20, 40, 60, and 80 s for three samples with the carrier concentrations indicated. The specific contact resistivities were calculated from non-mesa etched linear TLM patterns.

Annealing Time	20 s	40 s	60 s	80 s
1.4×10^{18} cm^{-3}	non-ohmic	non-ohmic	non-ohmic	almost ohmic
5.7×10^{18} cm^{-3}	non-ohmic	non-ohmic	non-ohmic	almost ohmic
1.5×10^{19} cm^{-3}	2.0×10^{-2} Ω cm^2	1.9×10^{-2} Ω cm^2	2.2×10^{-2} Ω cm^2	3.1×10^{-2} Ω cm^2

The high contact resistivities may be a result of a few causes. It is believed that the SiC may be depleted of carriers near the surface, possibly due to thermal oxidation. A depletion of carriers near the surface would result in higher than expected contact resistivity values because current transport across the contact depends on the carrier concentration in the SiC at the SiC surface. To investigate this potential problem we plan to compare the contacts described above with contacts on SiC implanted with Al and also on SiC which has not been thermally oxidized. The values of specific contact resistivity stated above should only be considered as preliminary estimates since only one level of the TLM measurement pattern was used. In the near future we plan to employ a circular TLM measurement structure [9], which consists of only one level and does not involve etching of the substrate. A photolithography mask for fabricating this structure was recently designed and fabricated at NCSU for this project.

D. Discussion

An Auger depth profile (Fig. 2b) of Ni/NiAl/SiC annealed at 1000 °C for 80 s shows that the surface oxide is thicker than that on the as-deposited sample (Fig. 2a). After sputtering for a couple of minutes, the O concentration dropped to below detectable limits; however, the data shows a decreasing Al concentration in the direction toward the SiC interface. This indicates that the kinetics are more favorable for the Al to diffuse toward the surface and react with O than for the Al to react with the SiC. Some of the Ni has probably reacted with Si at the interface to form a silicide, as indicated by the local maximum in the Ni intensity near the SiC interface, while the peak in the C intensity indicates the presence of an adjacent C-rich layer.

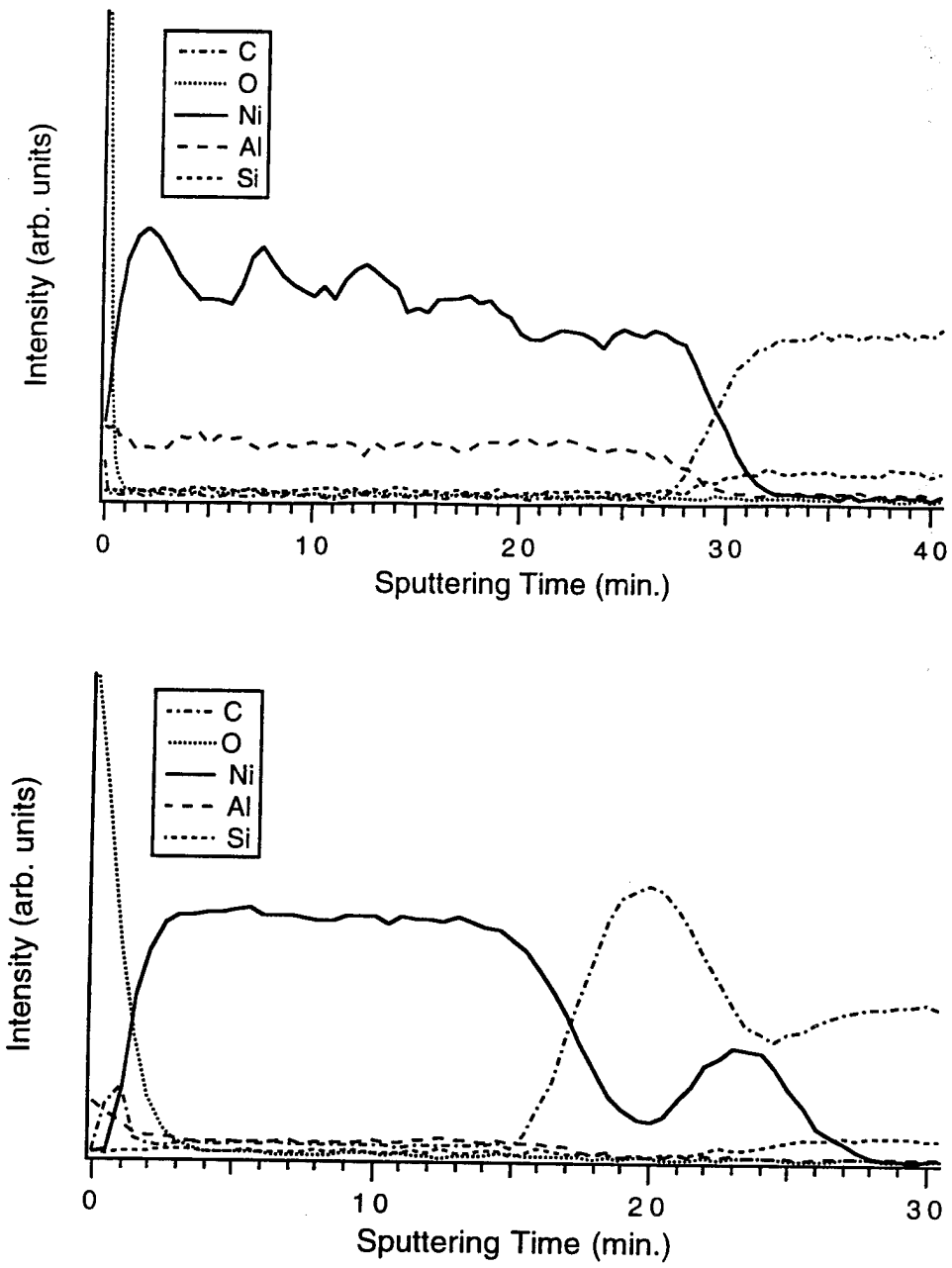

Figure 2. AES composition profile of (a) NiAl (1000 Å) deposited at room temperature on (0001) 6H-SiC and (b) Ni (1000 Å) / NiAl (1000 Å) / 6H-SiC annealed at 1000 °C for 80 s in N_2.

The demonstrated oxidation problem with Al necessitates the development of ohmic contacts which do not consist of substantial concentrations of Al. To reduce this problem we have chosen to investigate selected materials which contain B as an alternative to Al.

The main reasons for choosing B are that it is also a p-type dopant in SiC, its oxide is not as stable, and it is a much faster diffusant in SiC. Table II compares some important properties of B, Al, and their associated oxides. Although the B acceptor level in 6H-SiC is substantially

deeper than that of Al, the fact that B is an acceptor makes it worth investigating as a component in p-type ohmic contacts. Also, boron compounds tend to be more stable at high temperatures than aluminum compounds which suffer from the low melting point of Al. As shown in Table II, the diffusion coefficient of B is at least three orders of magnitude greater than that of Al. Therefore, more B than Al will diffuse into the SiC at lower temperatures. As discussed in this report, a major problem with Al-based contacts is the strong driving force for forming an insulating oxide layer. This situation is shown by the extremely low equilibrium partial pressure, p_{O2}, for Al_2O_3 formation. While B_2O_3 also has a low p_{O2}, it is significantly higher than that for Al_2O_3, indicating that the driving force for B to form an oxide is significantly lower. In addition, the melting point of boron oxide is notably low.

Table II. Selected Properties of B, Al, and Their Associated Oxides

Element	Activation Energy in 6H-SiC (meV)	Solid Source Diffusion, D_{SiC} @ 1800°C (cm^2/s)	Equilibrium partial pressure of O_2, p_{O2} @ 700°C (torr)	Melting temp. of the associated oxide, T_{melt} (°C)
B	700	10^{-11} [10-11]	10^{-35}	450
Al	240	$<10^{-14}$ [12]	10^{-47}	2040

Several boron compounds which possess reasonably low resistivities and high melting temperatures are listed in Table III. Of the compounds listed, the simplest to form by electron beam deposition would probably be CrB_2, VB_2, and ZrB_2. The refractory nature of these compounds increases the chance of forming ohmic contacts which will be stable at high temperatures.

Table III. Resistivities and Melting Points of Selected Boron Compounds

Compound	Electrical Resistivity (μΩ-cm) 298 K [13]	Melting Temperature (°C) [14]
CrB_2	30	2200
GdB_4	31	2650
MoB	45	2600
NbB_2	26	3000
TaB_2	33	3037
VB_2	23	2747
ZrB_2	10	2972

E. Conclusions

Nickel-aluminum was investigated primarily as an ohmic contact for p-type 6H-SiC because of the p-type doping of Al in SiC, the high melting point of NiAl (as compared to Al), and the tendency of Ni to form silicides but not carbides. This latter property potentially could have resulted in extraction of Si from the SiC lattice in exchange for Al, thereby enhancing the p-type carrier concentration at the surface. Although the I-V measurements indicate that some Al may be diffusing into the SiC after the longest annealing time performed (80 s at 1000 °C), this potential for reaction between Al and SiC appears to be exceeded by the driving force for Al to diffuse to the surface and react with O. A concentration profile obtained from AES analysis shows that Al has diffused through the 1000 Å Ni overlayer to form a thin (200 Å estimated) oxide layer.

In addition to the ohmic behavior resulting from annealing the NiAl contacts, as-deposited Ni, NiAl, and Au contacts deposited at room temperature on p-type ($N_A < 5\times10^{16}$ cm^{-3}) 6H-SiC (0001) were rectifying with low leakage currents, ideality factors between 1.3 and 2.4, and SBH's of 1.31, 1.27, and 1.37 eV, respectively. These results indicate that the Fermi level is partially pinned at p-type SiC surface, in agreement with our previous results on n-type SiC.

An alternative to Al for fabricating ohmic contacts to 6H-SiC is the use of boron compounds. The metal borides listed in Table III are strong candidates for p-type SiC metallization because their low resistivities and high melting temperatures should allow the formation of high temperature contacts. Electron beam deposition of these materials ought to be possible.

F. Future Research Plans and Goals

The position of the two crystal thickness monitors during simultaneous electron beam deposition needs to be optimized. First, the ratio of the actual thickness being deposited to the thickness read by each monitor needs to be determined. This can be accomplished by measuring the actual thickness deposited from familiar metal sources. With the completion of these system modifications to allow co-deposition of compound metal films, we are prepared to deposit B-based contacts as an alternative to Al-based metallization.

An attempt to fabricate ohmic contacts to p-type SiC using boron compounds will be made. The deposition of some of the low resistivity, refractory borides listed previously in Table III will be carried out by electron beam evaporation. Careful electrical characterization needs to be performed to determine if annealing will improve the contact properties. In addition, the deposited films will be chemically analyzed by Auger electron spectroscopy to determine if the proper phases form.

Another alternate approach to Al-based ohmic contacts for p-type SiC will incorporate p-type semiconducting interlayers. The goal of this approach is to find a semiconducting

material which has a favorable band lineup with SiC (i.e., reduce the band bending) and to which an ohmic contact can easily be made. We have chosen to examine the $In_xGa_{1-x}N$ system for interlayer materials because of the lower density of surface states (and hence less band bending) and the range of bandgaps over the composition range. It is planned to measure the valence band offsets and electrical characteristics between various compositions of $In_xGa_{1-x}N$ (starting with x=0) and SiC. If a low energy barrier at the interface results, metals will be investigated for ohmic contacts for the interlayer / SiC structure.

To extend the study on NiAl ohmic contacts for p-type SiC, the contact resistivities for annealing series at 1000 °C will be repeated using circular TLM patterns and two different substrates: 1) SiC implanted with Al to increase the surface carrier concentration and 2) SiC which has not been thermally oxidized to investigate whether the bulk carrier concentration can be maintained at the surface. A photolithography mask with the circular TLM patterns was recently designed and will be used in the research on ohmic contacts in the very near future.

G. References

1. D. Alok, B. J. Baliga, and P. K. McLarty, IEDM Technical Digest **IEDM 1993**, 691 (1993).
2. J. Crofton, P. A. Barnes, J. R. Williams, and J. A. Edmond, Appl. Phys. Lett. **62**(4), 384 (1993).
3. V. A. Dmitriev, K. Irvine, and M. Spencer, Appl. Phys. Lett. **64**(3), 318 (1994).
4. R. C. Glass, J. W. Palmour, R. F. Davis, and L. S. Porter, U.S Patent No. 5,323,022 (1994).
5. J. L. Murray, Ed. *Phase Diagrams of Binary Titanium Alloys* (ASM International, Metals Park, Ohio, 1987).
6. H. H. Berger, Solid State Electronics **15**(2), 145 (1972).
7. V. M. Bermudez, J. Appl. Phys. **63**(10), 4951 (1988).
8. T. Nakata, K. Koga, Y. Matsushita, Y. Ueda, and T. Niina, in *Amorphous and Crystalline Silicon Carbide and Related Materials II*, M. M. Rahman, C. Y.-W. Yang, and G. L. Harris, Eds., Vol. 43 (Springer-Verlag, Berlin, 1989).
9. G. K. Reeves, Solid State Electronics **21**, 801 (1978).
10. E.N. Mokhov, Y.A. Vodakov, G.A. Lomakina, Soviet Physics - Solid State **11**(2), 415 (1969).
11. C. van Opdorp, Solid State Electronics **14**, 613 (1971).
12. E. Mokhov, Y. A. Vodakov, G. A. Lomakina, V. G. Oding, G. F. Kholuyanov, and V. V. Semenov, Soviet Physics - Semiconductors **6**(3), 414 (1972).
13 Samsonov, G. V. and I. M. Vinitskii, *Handbook of Refractory Borides*, (Plenum Press, New York, 1980).
14. *Binary Alloy Phase Diagrams, 2nd Ed.*, T. B. Massalski editor, (ASM International, 1990).

VIII. Distribution List

Mr. Max Yoder Office of Naval Research Electronics Division, Code: 312 Ballston Tower One 800 N. Quincy Street Arlington, VA 22217-5660	3
Administrative Contracting Officer Office of Naval Research Regional Office Atlanta 101 Marietta Tower, Suite 2805 101 Marietta Street Atlanta, GA 30323-0008	1
Director, Naval Research Laboratory ATTN: Code 2627 Washington, DC 20375	1
Defense Technical Information Center Bldg. 5, Cameron Station Alexandria, VA 22304-6145	2